

Electro-Thermally Active Seal for Fast Response Tip Clearance Control

NASA Award Number: NNX15AR27A

Fanping Sun, Zaffir Chaudhry, Hailing Wu and Seung Bum Kim

United Technologies Research Center

February 28, 2017

This research has explored the concept of and validated engineering feasibility of electro-thermally activated variable geometry truss as a means of turbine blade tip clearance modulation. A sparsely populated wire truss actuation mechanism made of high temperature shape memory alloy can deliver an actuation with response time one order of magnitude faster than the current shroud contraction approach.

This report includes Phase I major findings and describes in detail the progresses made in Phase II since Sept 2015. The medium and high temperature shape memory alloy development was primarily conducted by Texas A & M University. Therefore, this work is summarized in the report and the full work report is attached in the Appendix.

Background

Actively maintaining a tighter blade tip clearance in aircraft turbine engine reduces hot gas leakage and offers promise of significant benefits in engine performance and operation economy such as fuel burn, pollution, life cycle and service life. Modern large transport engines use an Active Case Cooling (ACC) system that allows real-time modulation of turbine clearances, Figure 1^[1]. For most of the ascent and descent portions of the flight, the ACC is turned off; the engine runs with wider than desired clearances. At perceived steady-state conditions, a valve is actuated by the Full Authority Digital Engine Control (FADEC) to distribute cooling air around the engine, shrinking its case, resulting in tighter clearances.

The ACC system takes something on the order of a minute to reach full modulation of clearances. Due to the slow response rate, the steady-state clearance is mostly set to "more open" with respect to the possibility of snap throttle transients. For example, if the engine throttles were rapidly advanced to allow the aircraft to climb above localized turbulence, the resulting increase in rotor speeds and operating temperatures would cause the blades to "grow", reducing the amount of blade/case tip clearance. If the clearances were set tightly for maximum efficiency for the steady-state condition, there is potential for blade tip rub during and after the engine transient. The current means to allow for potential engine transients from a cruise condition is to back off on the steady-state clearances to provide margin against transients. The result is that the engine is not operating as efficiently as possible during long, steady-state flight segments, which dominate the overall commercial transport flight profile. On large transport engine, a tip clearance modulation of approximately 0.02~ 0.04 inches at rate of ~0.002 in/s would effectively solve the problem of unnecessary gas leak during cruise and improve engine efficiency significantly. Research has showed that a reduction of 0.01-inch in turbine blade tip clearance achieves about 1 percent improvement in specific fuel consumption (SFC) and approximately a 10 °C reduction in exhaust gas temperature (EGT)^[1].

In addition, the clearances are typically not uniform circumferentially around the engine. Engine-to-engine manufacturing variations and real-time load deflections tend to ovalize the case. Maintaining uniformly "round" clearances is important to extracting as much improvement in efficiency as possible. Therefore, an active clearance control system capable of locally independent modulation on a quadrant-by-quadrant (or smaller) basis to maintain circumferentially uniform clearances would have significant advantages over a single clearance

modulation device. Furthermore, the current ACC system makes it difficult for asymmetric clearance control, and heating/cooling air management is cumbersome^[2].

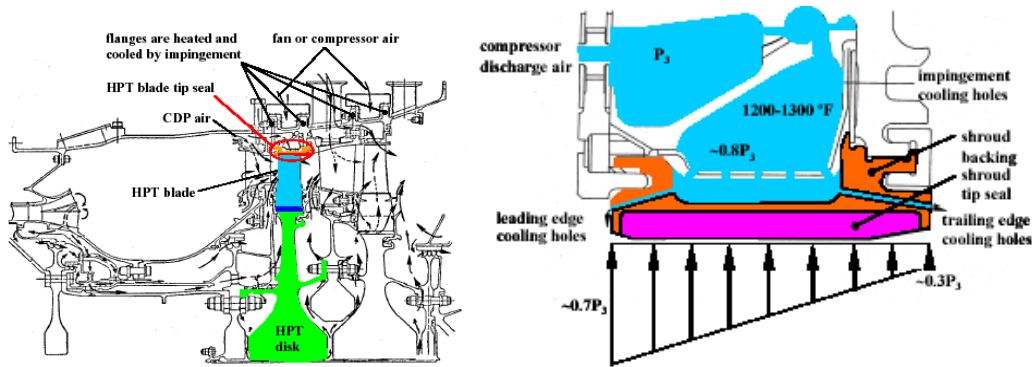


Figure 1 Current Technology—Thermal Expansion of Shroud
(Courtesy of Lattme’s Paper ^[1])

The primary reasons why the material thermal expansion has been the back bone concept for the turbine tip clearance control is the harsh and hostile environment and narrow cavity space surrounding the turbine blades. Over the past twenty years, a number of mechanical methods for rapidly modulating case clearance have been investigated ^[2, 3]. These include the use of magnetic bearings to axially displace the entire rotor fore and aft, as well as bladders or cinch straps to tighten the case about the blades. Each of these methods has proved to have drawbacks, typically relative to the precision with which the technology can position the case or rotor. In general, very few mechanical approaches having moving parts are considered viable for active tip clearance control. The temperature between gas turbine engine case and its shrouds typically exceeds 600°C, and the actuation mechanism must move the shrouds against large pressure differential (100~200 PSI) to increase or decrease the clearance in a short notice. Many research efforts have investigated active clearance modulation using axial or radial hydraulic and pneumatic as primary movers located outside of the hot section. More recently, research has shifted to solid state induced strain materials as the actuation muscles, such as shape memory alloy (SMA), piezoelectric and magnetostrictive. While most of them have still been proven less practical in temperature compatibility and integratibility into the shroud head room, recent work by NASA has demonstrated that SMA in wire form is by far the most promising clearance modulation muscle for its fast response, large actuation and compact design ^[4, 5]. Furthermore, the high temperature shape memory alloy (HTSMA) with phase transformation strain of 2~3% and phase transformation temperature from 200 °C to 400° C has been advancing rapidly and the some materials in useful product forms have become available for experimental evaluation and bench prototype^[6]. As the thermal clearance modulation is primarily hampered by slow response and small stroke, HTSMA, with large induced strain occurring at high temperature, appears to be opening door to a new design opportunity of turbine blade tip clearance control.

In summary, a means to rapidly, precisely and locally modulate the turbine case in response to a closed-loop feedback would enable significant improvements in turbine fuel efficiency and ultimately reduce emissions.

Key Approach and Technology Path

The objective of the research is to demonstrate the feasibility of fast response clearance modulation by high temperature shape memory alloy (HTSMA) as low thermal mass primary muscle in a hot environment of aero engine. As the HTSMA materials fully compatible with the turbine environment is currently still in development, the program is executed in two steps. First, we will design a variable geometry truss actuation mechanisms with extremely low thermal mass, no moving parts and integral to engine turbine shroud structure. We then use the state of the art medium temperature shape memory alloy (MTSMA, <400°C), originally developed by NASA and usable sample wire made available by university partner on the program team, as actuation muscle to evaluate the

concepts and performance in an elevated temperature environment. Second, we will identify/investigate a HTSMA (>600°C) material(s) and demonstrate its performances and feasibility for fabrication into usable forms, and then establish technology roadmap toward the ultimate implementation of the technology in turbine environment in the near future.

The fast response tip clearance control under research employs an intelligent variable geometry truss structure that is sparsely populated and possesses a very low thermal capacity. The active truss actuation structure, shaped in an annulus and suspending the turbine blade shrouds, or blade outer air seal (BOAS) to the engine case, consists of multiple segments, each individually controllable to its radial position, as shown in Figure 2. By resistive heating and air cooling its wire truss elements the actuator moves BOAS inward and outward to the engine center modulating the tip clearance in either linear or binary manner.

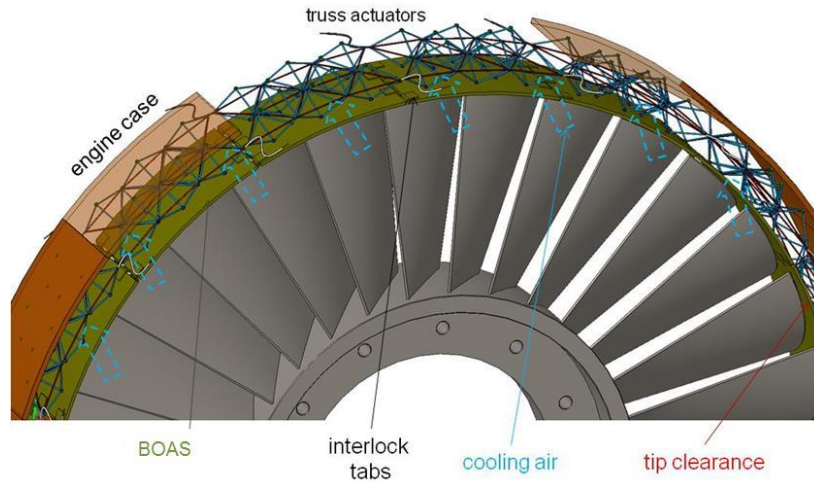


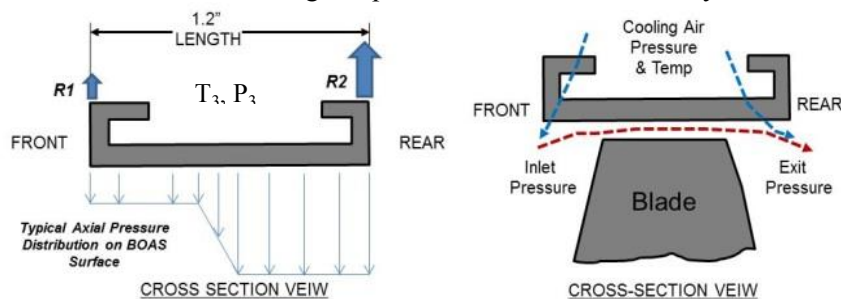
Figure 2 Tip clearance modulations by thermal truss actuation with low thermal mass

Design Requirement and Criteria

The notional design requirement for the active turbine tip clearance control of large commercial transport turbofan engines is as follow:

	Idle	Take off	Cruise	Decent	Max
P3, psi	55	550	200	35	650
T3, °C	260	677	510	232	732
R1, lbf	14	143	52	9	169
R2, lbf	23	231	84	15	273

Table 1 Derived design requirement metrics for ACC system [7]



This document does not contain any export controlled technical data

Figure 3 Load distribution and air cooling path of BOAS [7]

A first stage turbine of typical aero engine consists of 30~50 shroud segments surrounding rotor, often referred to as blade outer air seal (BOAS) to enable symmetric and asymmetric tip clearance control. Each is approximately 2.1x1.2 inches. The high pressure compressor bleed air (P_3) introduced in for cooling pushes BOAS toward blade tips, creating a large load on the actuation device which varies by flight segments. BOAS always have larger load at the rear hook (R_2) than at front hook (R_1). The actuator must be able to move BOAS approximately 0.02” upward and downward to open or tighten the clearance against the aero pressure and then retains its commanded position regardless the pressure variation. The material of the actuation must be compatible to the maximum temperature (T_3).

Operation Principle of Truss Thermal Actuator

The core structure of the clearance modulation device is a diamond-shaped, multi-strut truss element, commonly referred to as flextensioner. A two dimensional structure is analyzed here using simplified model, as shown in Figure 4, for its characteristics as an electro-thermal actuator. When all struts experience thermal expansion or contraction due to a temperature variation ΔT of air stream, a change Δy in the height of the diamond truss element occurs:

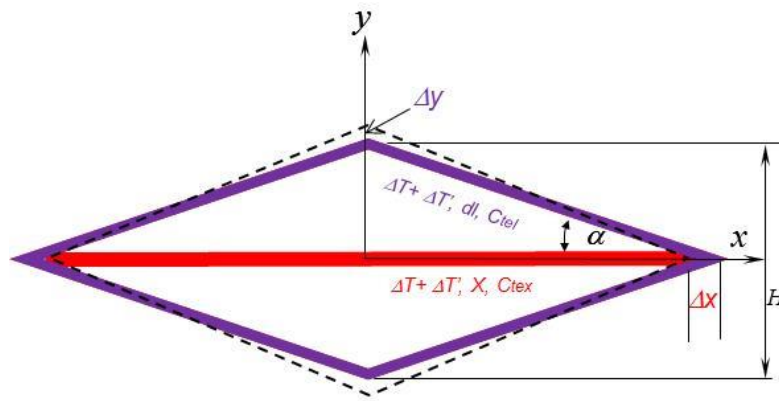


Figure 4 Operation principle of planer wire truss actuator

$$\Delta y = \frac{\Delta l}{\sin a} - \frac{\Delta x}{\tan a} = \frac{C_{tel}(\Delta T + \Delta T_l')l}{\sin a} - \frac{C_{tex}(\Delta T + \Delta T_x')x}{\tan a} \quad (1)$$

Where Δl and Δx are the thermal expansion of diagonal and the central strut respectively due to environment (airflow) temperature variation ΔT , and each strut's local temperature rise $\Delta T'$ induced by electric heating. C_{tel} and C_{tex} are their thermal expansion coefficients respectively. Δy is the displacement output of half of the actuator.

Equation 1 illustrates several interesting characteristics of such a diamond truss as an actuator. First, the thermal expansion of the central and diagonal struts contributes oppositely to the displacement Δy . The truss actuator then possesses a thermal environmental immunity, if the thermal coefficients of the diagonal and the central struts and the design angle α can meet the following criterion,

$$\cos^2 \alpha = C_{tel} / C_{tex} \quad (2)$$

Then the displacement Δy will remain zero regardless of the variation of temperature ΔT , or the actuation will not drift due to airflow temperature change.

Second, the thermal expansion of the diagonal struts or the central strut alone will generate displacement output when they are individually subject to temperature change ΔT

$$\Delta y = \frac{\Delta l}{\sin a} = \frac{C_{tel} \Delta T_l l}{\sin a} \quad (3)$$

Or

$$\Delta y = -\frac{\Delta x}{\tan a} = -\frac{C_{tex} \Delta T_x x}{\tan a} \quad (4)$$

When only the central strut x is heated or cooled, and the top vertex of the truss is fixed, then the total kinematic (rigid body struts) displacement of the actuator at the bottom vertex is

$$\Delta H = 2\Delta y = -2 \frac{C_{tex} \Delta T_x x}{\tan a} \quad (5)$$

Note that for the material phase transformation induced actuation under load, the net thermal strain output ε of the central strut becomes

$$\varepsilon = \Gamma - \sigma_x / E \quad (6)$$

Where Γ is the phase transformation strain under zero load, and it is a nonlinear function of the temperature change $\Gamma = \Gamma(\Delta T_x)$. The σ_x is the mechanical stress resulting from the external load on the strut (when it is constrained). E_x is the elastic modulus. Therefore, for SMA actuation, the total displacement output can be expressed as

$$\Delta H = -2 \frac{(\Gamma(\Delta T_x) - \sigma / E_x) x}{\tan a} \quad (7)$$

Equations 3 through 5 show that thermal expansions of the struts can be amplified by a factor of either $-2/\tan a$ or $-2/\sin a$. The amplifications are very close in magnitude for a small design angle α , but, are out of phase to each other. These features of a planer truss structure, that is, the ambient environment immunity, the structural amplification and phase control, could be very useful design configuration options and result in many benefits for actuators working in a harsh and demanding surroundings.

The displacement in Equation 7 is a kinematic and geometric calculation. Since each strut has a finite axial stiffness, the truss actuator thus formed is more compliant than the struts themselves when loaded, especially with a small design angle. The equivalent stiffness at the output vertex can be defined as

$$K_y = \frac{F_y}{2\Delta y_y} = -\frac{K_l K_x}{\frac{K_x}{\sin^2 \alpha} - \frac{2K_l}{\tan^2 a}} \quad (8)$$

Where, F_y is the vertical load, $K_l = E_l A_l / l_l$ and $K_x = E_x A_x / x$ are the diagonal and central strut stiffness respectively, E and A are the elastic modulus and the cross section area for each strut, respectively.

For instance, if we select a pair of materials for the struts that meets $C_{tel} / C_{tex} = 0.98$, and design the angle $\alpha = 15^\circ$, the linear thermal expansion by ambient temperature change ΔT in all struts would generate zero net displacement at the output vertex regardless of temperature variation. Meanwhile, the phase transformation induced strain Γ by electric heating ΔT_x works independently to yield a controlled actuation output ΔH . That could make a

temperature drift-free actuator ideal for engine turbine with a wide range of operation temperatures (Table 1). Also we can choose to active the diagonal struts for in phase control, or the central struts for out of phase control.

The thermal expansion of the central strut in this example is amplified by a factor of 7.4. Obviously, by the principle of virtual work conservation, its amplification is at the cost of load capacity. The smaller the design angle, the larger the amplification and the lower the stiffness. Therefore, as a clearance control actuator requires both large displacement and substantial load carrying, the design is a compromise and optimization among the two requirements. Highly loaded actuation demands larger design angle α , and a large displacement needs a small design angle. Figure 5 shows the relative stiffness and structural amplification vs the design angle with axial stiffness ratio of the diagonal and central struts as a reference variable. In the later designs, a design angle around 30° is always employed.

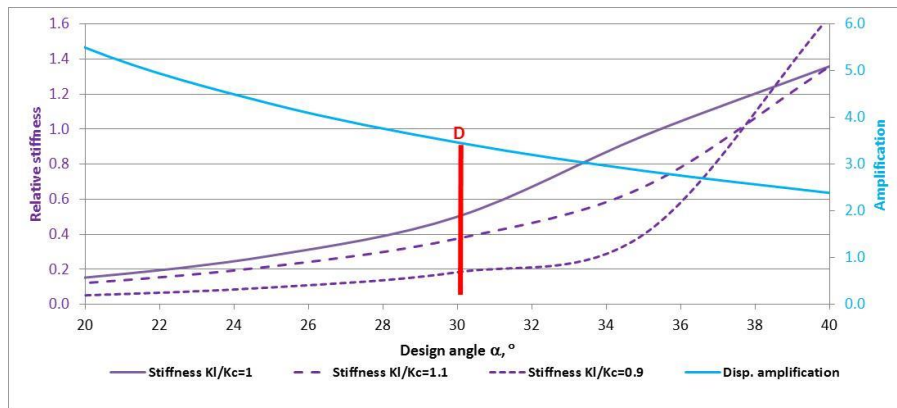


Figure 5 Displacement amplification and relative stiffness of the truss actuator, D is the current design point.

Prototype Design and Analysis

The major evolution of LEARN Phase II from Phase I is the design philosophy shift of the actuation mechanism from thick strut (rod) based truss to thin wire based truss. A truss actuator with thin wire as muscle always under tension has many advantages. It overcomes the enormous challenge of pre-stressing thick truss elements encountered in Phase I experiment and can substantially increase the effective strain recovery from SMA phase transformation. The thin wires also enable resistive heating of entire actuation mechanism without complex and awkward power distribution system. It eliminates many unnecessary electric junctions and avoids overheating the remaining electric junctions, as the resistivity of the electric junctions are typically greater than that of the struts element. The local overheat could become so bad that it largely changes the desired truss heating pattern and temperature distribution along the struts and therefore grossly reduces the output actuation displacement. In phase II, we have down selected two among many conceived thin wire based actuator concepts for detailed analysis and prototyping. The first one was predicted by the models as a great design in terms of the structural and electric simplicity and the potential for low cost mass production by stamp forming and tack welding. The modeling effort is a success, establishing an integrated FEM/CFD thermo-fluid-structural modeling tool in COMSOL platform that is applicable to the second concept analysis. However, the prototyping has encountered many practical issues in fabrication and assembling requiring special precision tooling and fixtures which is not practical within the scope of the current program. The concept was therefore shelved after a quick and crude experiment. The second concept has succeeded in both prototyping and experimental and analytical validation. Both concepts are reported in the following sections.

System Design I- Interwoven Wire Mesh Truss Actuator

The first design is shown in Figures 6(a) and (b). A three dimensional interwoven truss mesh made of diagonal SMA wires (a) forms an active variable structure linking the engine case to BOAS (b) at its vertices. The truss actuator consists of active wire segment only and the all central struts are inactive (part of the engine case and BOAS, as in Equation 3). The truss mesh is pre-strained by the combination of pressure differential across BOAS and compression springs (not shown in Figures 6 but in Figure 10). When all serpentine wires contract diagonally when resistively heated from Martensitic phase to Austenite phase, they lift BOAS and widen the blade tip clearance. The wires return to original length by pressure and spring load after the heating power is removed and the wires are cooled by ambient airflow below Martensitic start temperature M_s .

Three sets of SMA wire in the mesh are anchored to the engine case (top) and BOAS (bottom) respectively at their vertices by bolts. They are electrically insulated at the anchors to each other and collectively suspend BOAS against the load. The two wire sets (red and blue) run in parallel with vertices anchoring configuration opposite to each other. The third set (green) lies perpendicularly without interference to the other two wire sets at any crossing points. This 3D interwoven mesh configuration maximizes the actuation authority and can be made extremely compact to fit in the narrow head room over turbine BOAS. Each set of SMA wires can be electrically connected in series to reduce the actuation current and losses in the connections. They can also be individually powered to generate a desired level of clearance modulation. The wire mesh is preloaded in tension by four compression springs (Figure 10) at each corner of the BOAS respectively. This design could enable more discrete clearance control rather than binary SMA actuation and eliminates the need for electric insulation at each wire crossings/attachments. As it is a diagonal wire actuation, the displacement and amplification design follows the rules of Equations 3 and 5.

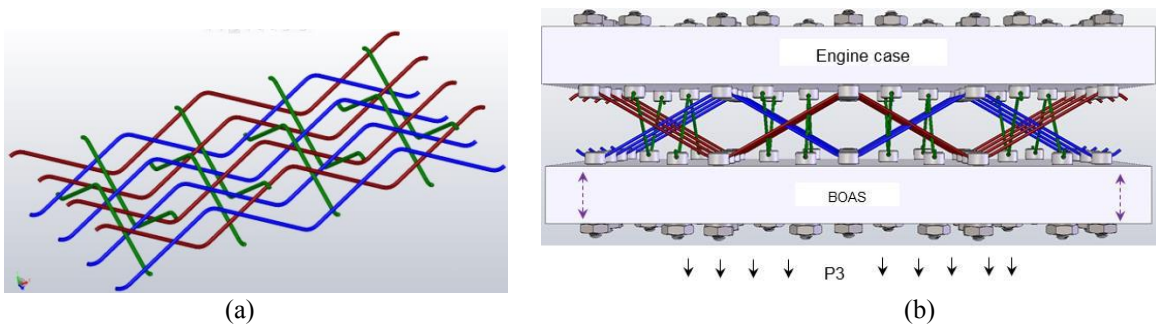


Figure 6 SMA active truss clearance modulation system and the interwoven SMA wire mesh.

Integral Thermo-Fluid-Structural Modeling

A comprehensive multiphysics model is created to evaluate the design and to conduct the system/component optimization. The model takes the electric power as input to SMA wires and the actuation displacement of BOAS as output. The model calculates the displacement and load performance with cooling airflow, structure heat transfer and SMA material properties all coupled.

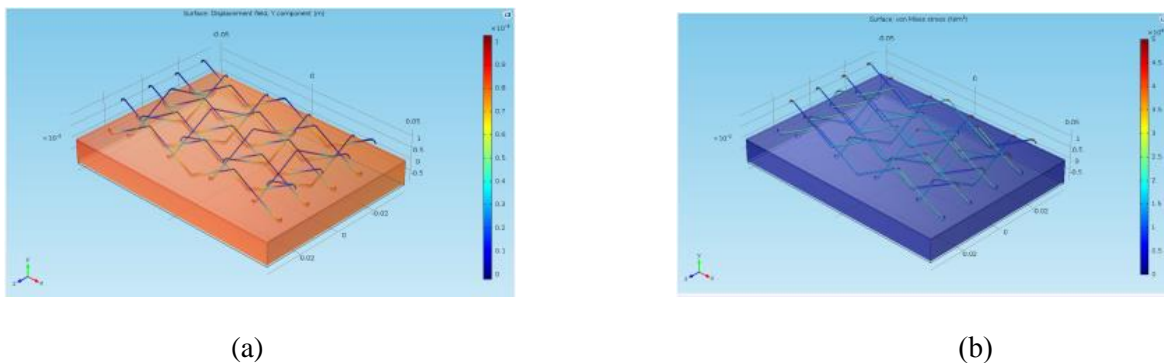


Figure 7 Structural analysis of wire actuator, (a) truss displacement field, (b) truss stress field @150lb load/BOAS

The structural analysis with COMSOL model has validated that the actuation by 2% induced strain of the SMA wire truss can deliver a nominal displacement of 0.02". The triangular configuration of the truss amplifies the induced strain of SMA wire by a factor of 1.8. The 0.02" diameter wire truss is also cable of suspending BOAS against the load with its combined maximum stress well below the material strength limits, as shown in Figure 7.

The thermal response time of the truss, cooling airflow requirement and the corresponding heating power are the most critical design criteria and evaluation matrices for rapidly widening the clearance. To investigate the coupled electric-thermal-fluid-structural characteristics, a conjugated heat transfer COMSOL model was developed to examine the thermal behavior during the resistive heating and air cooling of the wire truss. The model simulates activation and deactivation time and temperature profiles of the wire truss when air of ambient temperature constantly impinges the wires. Figure 8 illustrates simulation of the transient temperature during heating and cooling for conditions in consistent with a commercial available Nitinol SMA wire ($A_f \sim 100^\circ\text{C}$). With large cooling airflow of ~ 10 m/s, 80 watts electric power heats the wire mesh well beyond its full activation temperature of 120°C (20°C above its nominal A_f) in 2 seconds. For a small air flow of 0.1 m/s, the heating only takes 1.4 seconds.

When the electric heating power turns off, the same 10 m/s airflow cools the wires to 60°C , a temperature well below its Martensitic start M_s 90°C , in 12 seconds, thus completing an electro-thermal actuation cycle. This validates that the thermal activation and deactivation cycle is dictated by thermal mass of the truss mesh and the cooling airflow. The air cooling can be completed at response speed at least 5 times of the current prevalent active case cooling (ACC) tip control system (>60 second). The continuing rise of the wire temperature beyond the activation temperature indicates that more than sufficient heating power is applied in an effort to accelerate the activation, and therefore, to avoid the overheating of the wire without slow down the activation, and also reduce the power consumption during the temperature holding state, it is necessary to optimize electric power input profile with a PID control and temperature feedback.

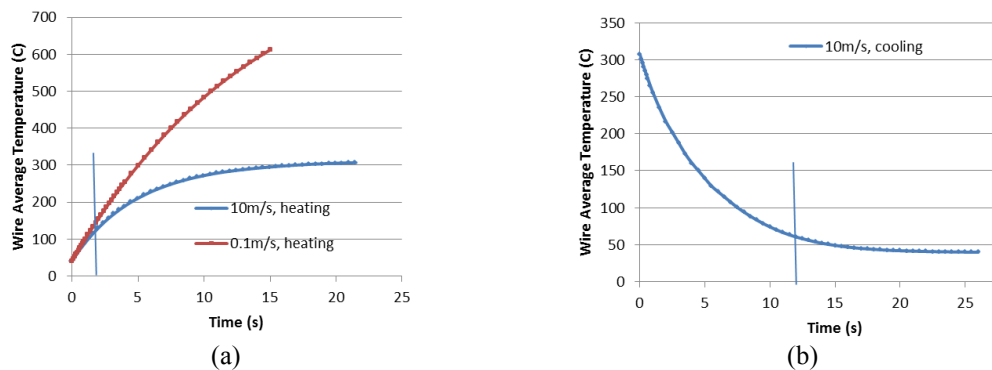


Figure 8 Transient wire temperature, (a) resistive heating with 80 Watts power, (b) cooling with 40°C air and zero power.

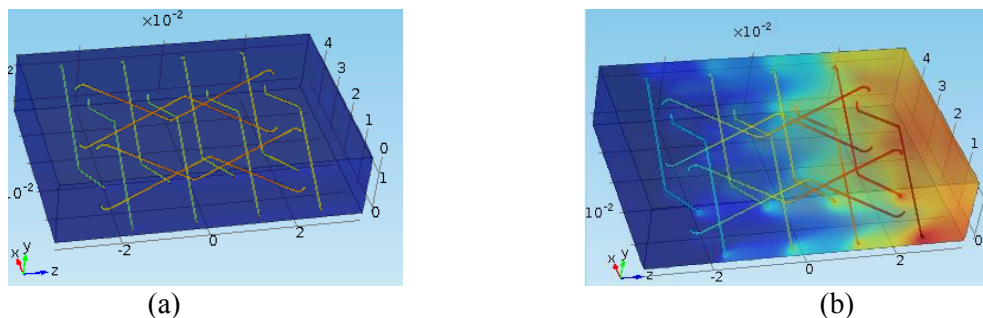


Figure 9: Comparison of steady state wire temperature and spatial temperature distribution in the wire mesh actuator at different cooling air velocities, (a) 10 m/s, (b) 0.1 m/s, air temperature 40°C .

Figure 9 illustrates steady state temperature of the truss wires and their spatial variation due to their orientation with respect to the cooling airflow and their location along the airflow path. Cooling air velocity has a strong effect on the heat dissipation from the wires and temperature uniformity of the wire mesh. It is depicted that a high air velocity generates a fairly uniform temperature field within the actuator cavity. As the airflow speed decreases to almost stagnant (0.1 m/s), the wire and air temperature as well as temperature spatial variation greatly increases. This indicates that a large airflow is desirable not only for the fast cooling (fast de-actuation response) but also enhancing temperature uniformity and wire reliability and durability, as the minimal heating power is dictated by the lowest temperature spots on wires in order to ensure uniform and complete material phase transformation and maximize strain recovery of SMA. This is, of course, at the cost of heating power consumption.

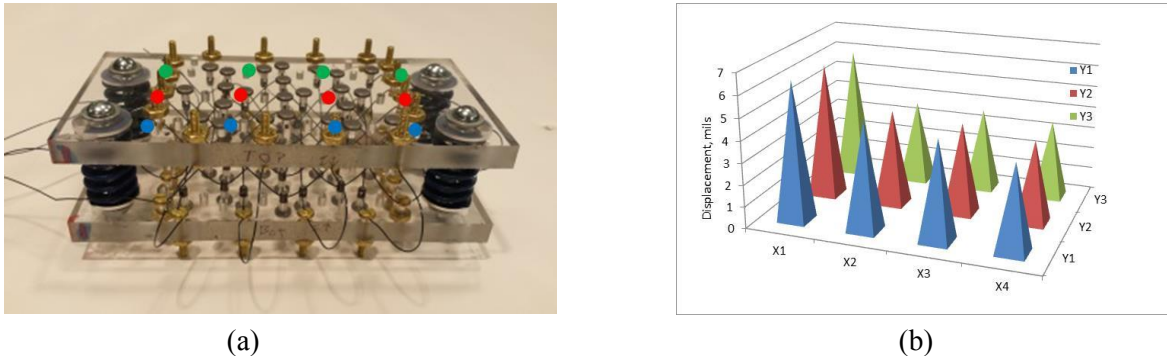


Figure 10 Prototype of interwoven wire mesh truss, and displacement measurement. The dots are the locations of each measurement.

While awaiting the MTSMA to be hot rolled and drawn to useful wire by the university partner and vendor, we have quickly made a proof-of-concept prototype of the concept, shown in Figure 10(a). The prototype employs low temperature Nitinol SMA ($A_f \sim 100^\circ\text{C}$) available off the shelf to simply evaluate kinematics and reveals structural feasibility and manufacturability of the concept. Although the concept and models illustrate great promise in the performance such as displacement of BOAS, actuation speed and simplicity of resistive heating, the measurement of BOAS displacement shown in Figure 10(b) reveals some deficiencies of the design. In a presumed full activated state, the SMA wires are heated above $A_f \sim 100^\circ\text{C}$ and an airflow of approximately 2 m/s velocity is blown between two plates along the length of the actuator, only 0.0064" motion was observed at one corner of the BOAS by non-contact laser displacement sensor while the model predicts 0.020". In addition, BOAS plate is highly tilted toward one side. A displacement of 0.0036" was measured at the diagonally opposite corner. Furthermore, the actuation is not very repeatable, indicating the mechanism possesses large friction and hysteresis.

Further analysis reveals that major cause of the gross loss of the clearance motion is the "slack" in serpentine wire mesh at the each anchor point. Each SMA wire is anchored to the BOAS by a series of bolts through small holes on them. The SMA wires, although small in diameter (0.02"), does not conform to the holes' cross section well because of its bending stiffness and insufficient tension applied to the wires by the preloading springs. As a result, the wires bend at the anchors with a fairly large radius. When the wires contract upon heating, they are pulled more "tight and straight" and the bending radius decreases. As a result, the large percentage of the wire contraction could be thus absorbed by the radius change at anchor points and only a small portion of motion is actually transferred to the BOAS. A secondary cause appears the non-uniform heating of the wires, resulting in their asymmetric contraction of each triangle wire segment between anchors and then consequently the hysteresis and non-uniform BOAS actuation. These manufacture problems could be addressed by either using bundle of very thin wires with less overall bending stiffness, or greatly increasing the bias spring load. However, it is anticipated that these solutions may end up hurting stroke output and load carrying capability in another way, because multi-strand twisted cord has less effective tensile stiffness and larger bias will reduce the displacement output. Wire bundle could make the manufacturing process even more complicated and the overall performance less predictable. Also the complicated and continuous serpentine wiring and 3D interwoven mesh could cause

reliability and maintenance issues in engine hot section environment. Furthermore, the mesh wires works diagonally. It widens up the clearance upon power heating and tightens when cooled (out of phase), the requirement of failsafe in the event of electric power loss demands either separate mechanical position latch or a backup power supply, which adds more complexity to the actuation mechanism.

System Design II Actuator with Flextensioner and Straight MTSMA Array

With all the learnings from the first prototyping, we decided to change the design philosophy of wire configuration. Instead of wiring the SMA in zig-zag form, which makes them carry out three functions in single component, the new design separates the actuation muscle, SMA wires, from motion conversion and amplification functions. It employs a standalone structural frame, commonly referred as flextensioner, as shown in Figure 11. In this design all the actuation muscle wire segments are retained in the same plane (or staged for better air cooling purpose) and straight form. Mechanically all the SMA wires act in parallel to enlarge the load carrying capacity. Electrically they could be connected in series through external jumpers, thus preserving the benefits of low current resistive heating (SMA wire has extremely low electric resistivity). The flextensioner functions as motion amplification and conversion from tangential direction to radial direction.

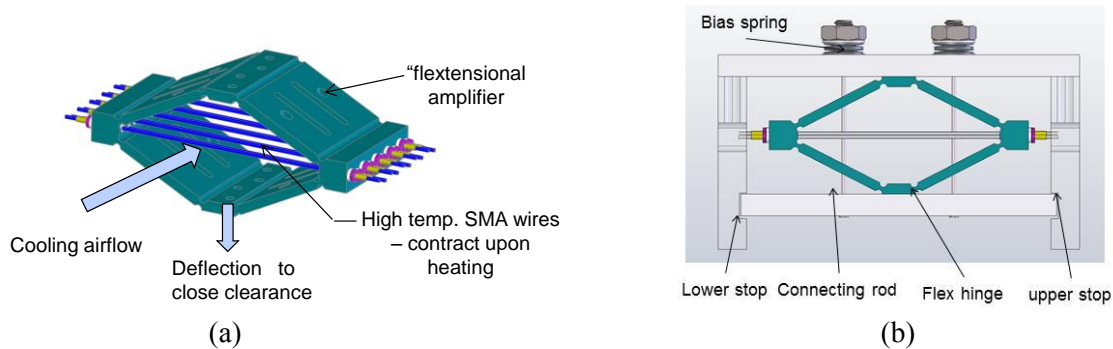


Figure 11 Flextensional SMA truss actuator and assembled clearance modulation device, (a) actuator alone, (b) clearance modulation assembly.

The new clearance modulation actuator consists of a flextensional amplifier and ten straight SMA wire segments connecting the two ends in parallel along the longitudinal axis of the flextensioner. The 2-D flextensioner consists of four strut plates joined together via eight flexal hinges at its four end pieces respectively. It is made of stainless steel and cut out in one piece by electric discharge machine (EDM). The flexal hinges provide rotational freedom without friction and release the bending stress to each plate. Each plate acting like a strut only subject to compression or tension. The complexity of the structure shape and its frictionless hinges is very much offset by its one-piece design and fabrication via EDM. The SMA wire segments are retained and biased by the spring stiffness of the flextensioner during assembly to eliminate slacks. For fewer electric connections and more reliable wire termination, all ten wire segments are actually assembled in five U-shaped pairs (Figure 20). Each pair is with a U-shaped stainless steel tube on one end and two crimped straight tubes on the other free end. The wires are insulated from the flextensioner by machinable ceramic bushings and glass epoxy washers. The five wire pairs are electrically connected in series to form a single circuit for resistive heating by a DC power supply.

The cooling airflow directly impinges the SMA wires perpendicularly. The thermally induced contraction and expansion of the wires are converted to the structural deflection of the flextensioner in the direction perpendicular to the wire set plane, as shown in Figure 11(a). As the top of the flextensioner is mounted to the engine case (Figure 11(b)), the bottom moves BOAS up and down changing the tip clearance setting. The mechanical stops at the top and the bottom of the clearance range are built in to limit the BOAS motion. In conjunction with the inherent nature of SMA's binary actuation, the clearance modulation device is designed to toggle BOAS between two extreme positions, that is, the maximal clearance during the take-off, climb, approaching and landing to avoid rubbing, and the minimal clearance during the cruise for fuel efficiency.

The actuation (clearance increase) and deactivation (clearance decrease) cycles as follows:

1) In the turbine head room cavity, there is an airflow from the high pressure compressor that constantly blows to cool the BOAS. A portion of the airflow is now redirected to impinge the SMA wires array of actuator. The SMA wires are in power off mode, BOAS is being held in its upmost position by the bias spring against the upper mechanical stop.

2) A large current quickly heats up the SMA wires above its phase transformation temperature (A_f , 240°C for MTSMA, Hafnium wires). The wires contract and the flextensioner moves BOAS downward to its target clearance until stopped by the lower mechanical stop. The current is then reduced by the controller to a level that is just enough to sustain the heat flux equilibrium between the wires and airflow, thus to preventing BOAS from drifting upward and slowly returning to its origin by the bias spring load.

3) When the current turns off, the heat flux equilibrium breaks. The SMA wires are now quickly cooled by the same airflow to a temperature below its phase transformation temperature (M_s , 190° C for MTSMA) and extended by the bias spring. The flextensioner returns BOAS back to its upmost position and completes a binary actuation cycle.

For a given ambient air temperature in the turbine BOAS head room and actuator thermal inertia, major consideration of the design is given to a balance between airflow velocity and heating power. High airflow velocity with lower temperature tightens clearance faster at cost of more heating power during the longest flight segment. Low airflow velocity reduces the actuation response time but consumes less electric power. High airflow velocity also slows down the heating up and delays the tightening of clearance. Fortunately the rate of clearance closure is not a critical requirement. In addition, a constant load spring is preferred in order to maintain a flat bias. The ideal clearance modulation device should not be subject to the air pressure variation during the cruise flight segment.

Figure 12 notionally illustrates the entire tip clearance modulation system with multiple actuators and BOAS interconnected circumferentially. Each BOAS is linked to its two adjacent neighbors through flexible leaf springs/air seals. This allows for some independent movement of each BOAS when driven by the actuator at its center, and enables asymmetric clearance compensation. All actuators can be powered individually or collectively through their electric connection points to achieve symmetric and/or asymmetric modulation.

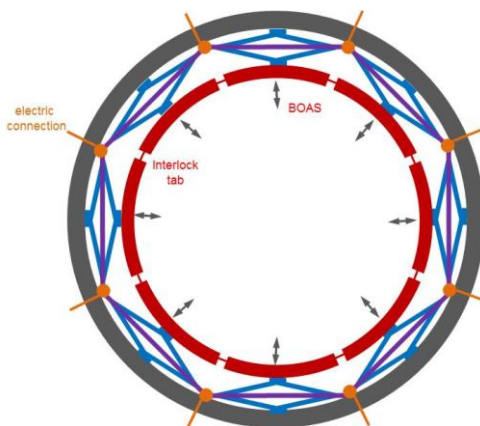


Figure 12 multiple actuator and BOAS configuration

The backbone of the actuation is the SMA wires that undergo material phase transformation by thermal cycle. Figure 13 shows the stress/strain relation of the MTSMA wires ($Ni_{49.2}Ti_{35.5}Hf_{15}$) in two material states. The operation line (stiffness) of the flextensioner actuator is overlaid on top of it. The SMA wires are restrained by the flextensioner (and bias springs) to operation point B during the assembling and setup. B is the base operation point with SMA wire in Martisite state (low temperature). A is the operation point with SMA wire in Austenite state (higher temperature). Upon resistive heating over the phase transformation temperature A_f , the wires contract to point A from point B and yield a net 1% decrease in strain and 200 *Mpa* increase in stress. The net

strain change of the wires are then collectively converted and amplified to radial deflection by the flextensioner. When the power is turned off and wires are air cooled to below the Martensite start temperature M_s , they are stretched back by the spring force of the flextensioner to their original length. The operation of the actuator is a flip-flop cycling between B and A initiated by the resistive heating of the wires and forced air cooling, respectively. As the difference between M_s and A_f is typically small, retaining the SMA wires in an intermediate strain is nearly impossible.

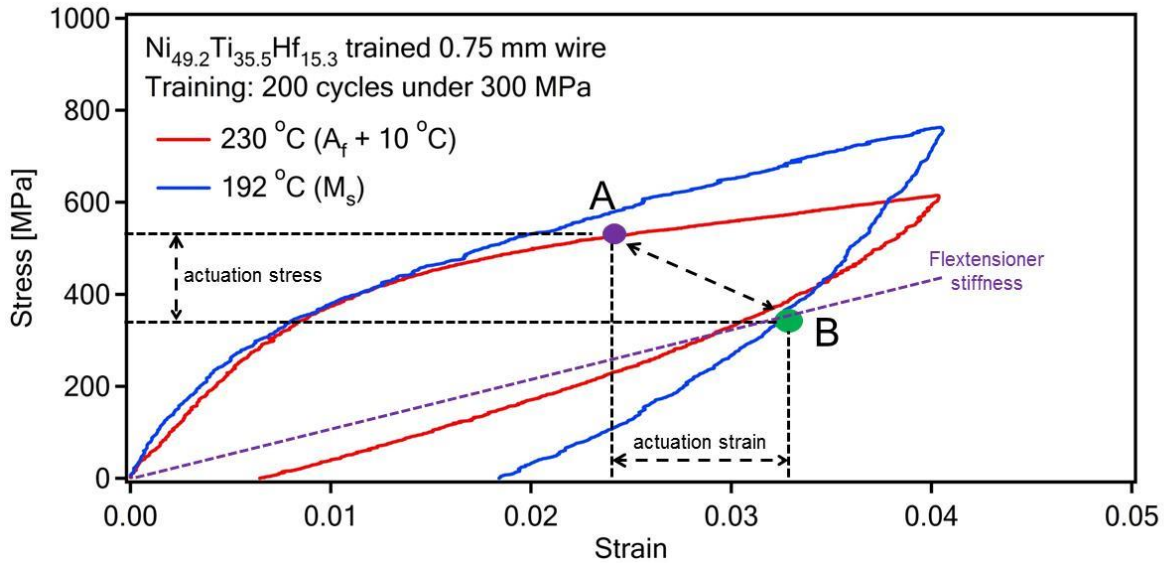


Figure 13 Strain and stress relation in two material phase states and operational design of the actuator, MTSMA wire, Ni_{49.2}Ti_{35.5}Hf_{15.3}, 0.030” in diameter.

Multiphysics Modeling

The new design is analyzed by the multi-physics model in COMSOL to estimate the performance, Figure 14. With 1% thermally induced strain input to the SMA wires, the flextensional SMA actuator is capable of 0.035” deflection against a load of 120 *lb*/BOAS. The stress in the wires at fully contracted and loaded mode reaches 50% of the allowable stress (40*ksi* for repeated operation of the MTSMA). The maximal stress in the flex hinges are well below the allowable of the material (SS303).

The CFD and heat exchange model predicts that a de-actuation time, or the time to cool the wire from above Austenite finish (A_f) temperature 300°C to below Martensitic start temperature (M_s) 150°C, is approximately 12 seconds. The airflow velocity is 10 m/s and ambient temperature 110°C, see Figure 15. The CFD models also reveal uneven cooling of the wires along the airflow path, shown in Figures 16 and 17. At a high airflow, the first two wires near the air nozzle directly impinged by airflow are “quenched” at much higher rate than those in the wake of the preceding wires. Downstream in the far field of the airflow, the temperature spatial variation starts to decay. This uneven temperature distribution among wires and along each wire can result in a reduced effective actuation in both force and displacement and demands more electric power to activate. At a slow airflow, the heating uniformity becomes worse. This has resulted in a change in SMA wire configuration from all-in-plane to slightly staggered design.

The models confirm that the objectives of a clearance modulation of 0.02” motion and one order of magnitude faster response time than the conventional active case cooling (ACC) is feasible.

NARI LEARN Fund – Final Technical Report

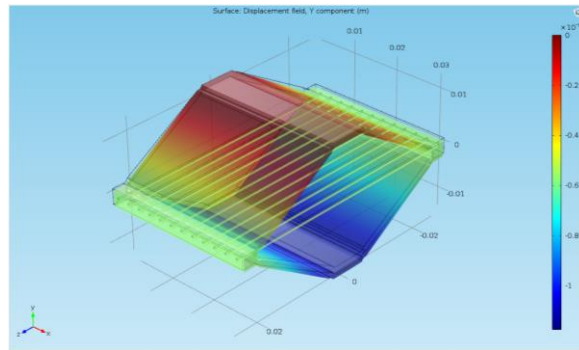


Figure 14 Structural deflection during actuation (wire heating)

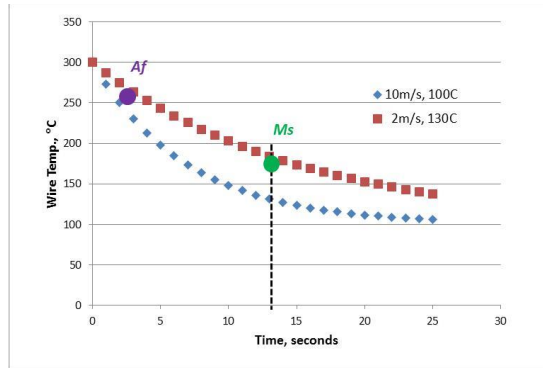


Figure 15 Wire temperature decay by cooling airflow during deactivation

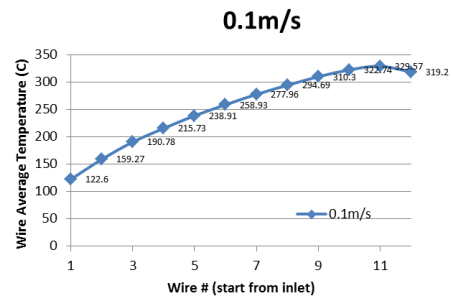
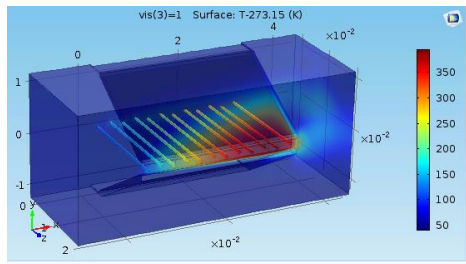
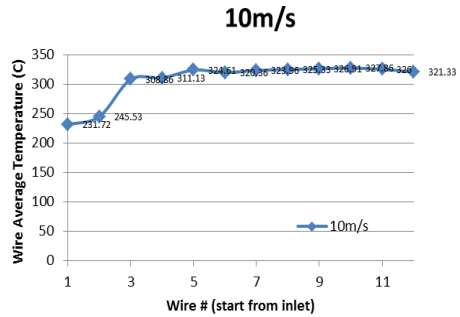
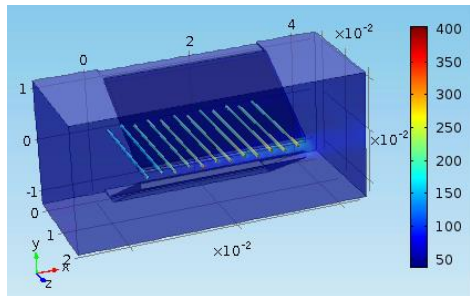


Figure 16 Spatial temperature variations by cooling airflow during deactivation

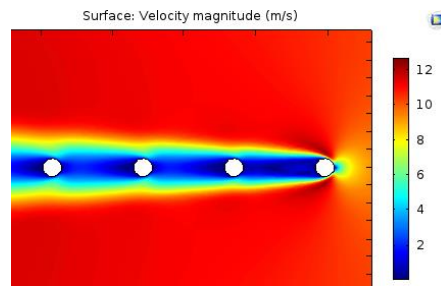


Figure 17 Effect on wire cooling by direct impinging airflow and in the wake of preceding wires

Fabrication of Flexensioner Actuator with Straight MTSMA

The actuator consists of a stainless steel 303 flexensioner and five pairs of MTSMA (Ni49.2Ti35.5Hf15) wires. The assembled actuator is shown in Figure 19. The each wire pair segments are terminated by a U-shaped stainless steel tubes on one end and by two crimped straight tubes on the other end, as shown in Figures 19 and 20. In addition, the straight tubes are tack welded to the SMA wire ends to further straighten the shearing resistance. The wires are insulated from the flexensioner by machinable ceramic bushings radially and glass epoxy washers axially. The five wire pair is electrically connected in series to form a single circuit for resistive heating by a single DC power supply. The MTSMA alloy developed by Texas A&M University are hot rolled into ~0.19” diameter rods and then cold drawn to 0.030” wires by other special metal processing shops.

The major issue encountered during the fabrication of the actuator was SMA wire termination. The termination of SMA wires has historically been a challenge. The challenge is augmented by the fact that the newly developed MTSMA is more brittle and harder than conventional Nitinol SMA. To retain full strain recovery from SMA wires, the termination must hold high shear stress without any slipping regardless of the temperature cycling, differential thermal expansion and stress alternation. In our design, a 50 *lb.* shear force is expected on a 0.03” OD wire and a connection length of 0.25”, resulting in over 2100 psi shear stress. Many approaches were evaluated and experimented such as spot welding; brazing, soldering, and SMA shrink tubing. None of them had worked long enough to complete a few testing cycles before the wire ends either slipped or fractured, as shown in Figure 21. The success of the termination shown in Figure 20 attributes to a few measures: 1) the U turns on one end of the actuator reduces the number of joint termination (as well as the probability of failure) by 50%, 2) clearance between tube and wire were kept very tight (0.001”), and 3) the deep crimp of the straight tubes creates double bend with tiny radius. Along with the tack welding of the wire end to the tube end. The combined effort of “Euler's rope friction, the structural bending stiffness of the wire and tube makes a very robust termination.

The second challenge in the fabrication was electric insulation. The insulation step bushings made of machinable ceramic were easily fractured or crashed during the assembly and during the testing, causing bushing replacement and reassembly of the actuator many times. The reason of this failure is still not clear as the estimated compression stress inserted on the bushes is well below their allowable. We finally replace them with glass epoxy washers for axial load and insulation, and use the same ceramics bushing for radial insulation only. They never fail again. Although the maximum temperature of glass epoxy is lower than the ceramic, it is adequate for the testing with MTSMA below 350 °C. For the HTSMA > 600°C, and engine implementation, a solution of high strength and high temperature must be sought.

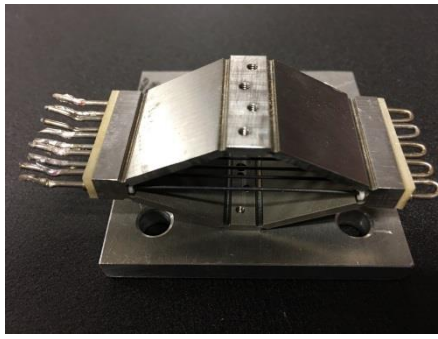


Figure 19 MTSMA ($\text{Ni}_{20}\text{Ti}_{40}\text{Pd}_{30}\text{Hf}_{10}$) actuator assembly

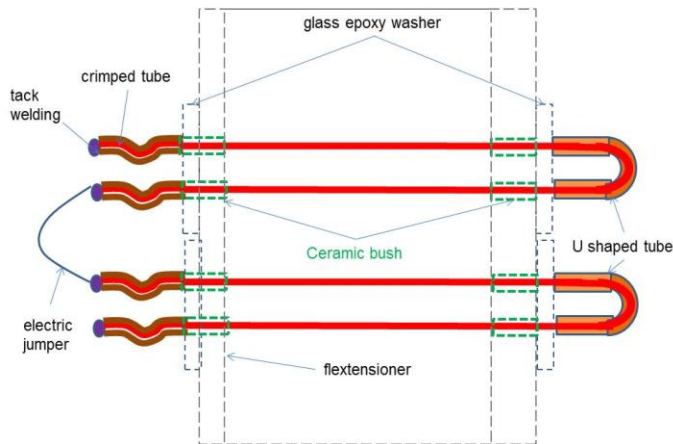


Figure 20 HTSMA wire termination that holds the load w/o slipping.

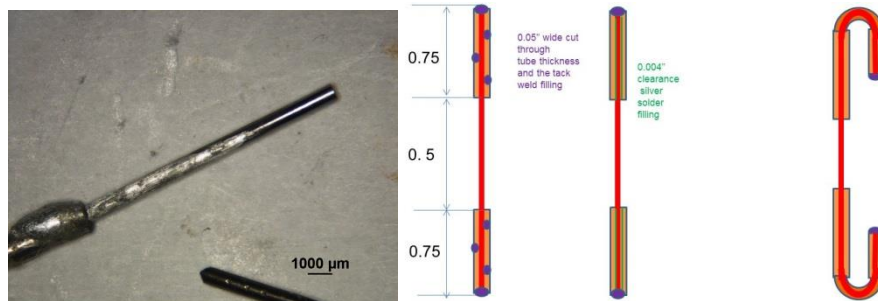


Figure 21 MTSMA terminations that failed, from left: high temperature soldering, tube welding, and elbow bend welding.

The HTSMA 0.030” wires used are fabricated in the following process. $\text{Ni}_{49.2}\text{Ti}_{35.5}\text{Hf}_{15.3}$ alloy was hot extruded at 900°C in order to obtain the input material for the final wire drawing process. For this purpose, the as-cast $\text{Ni}_{49.2}\text{Ti}_{35.5}\text{Hf}_{15.3}$ alloy bar with a diameter of 12 mm was hot extruded at 900 °C to obtain 2 mm thick wire. The material was jacketed in stainless steel in order to protect the material from oxidation at elevated temperatures, and it was removed upon achieving a 6:1 reduction in diameter.

Experimental Validation

A test apparatus was built to evaluate the MTSMA actuator in a simulated hot and pressurized section of a turbofan engine, as, shown in Figure 22. The experimental setup consists of a programmable hot air blower (Leister Hotwind System), a hot air actuator test chamber, a programmable DC power supply, instrumentation

conditioners and a data acquisition/controller system. The controller can set up the test conditions, such as cooling airflow speed and temperature and control electric power input to the actuator. The hot airflow is directed via a duct to the hot air chamber. The hot air impinges the MTSMA wires of the actuator with a thin air sheet from the back of the chamber through a rectangular cross-section nozzle and exits at the full open front end to ambient. The hot air blower is variable speed (up to 25 m/s) and variable temperature (up to 500°C).

The hot air test chamber, shown in Figure 23, is equipped with four sets of nonlinear Belleville spring stacks which preload the actuator evenly via four pull rods to an appropriate bias level (point B in Figure 14). It can also mimic the air pressure load, by adjusting the bolts on the Belleville springs, and to maintain a relatively constant load through the actuation cycle. The total load on the actuator is monitored by four load cells on the top of the device right below the Belleville stacks. The movement of the actuator and BOAS is sensed by four eddy current non-contact displacement sensors below the BOAS plate. Because of the large size of the BOAS relative to its contact area with the actuator, the uneven movement of the BOAS was anticipated; four load cells and four displacements are employed to monitor the uniformity and spatial variation of all measurements, one at each corner of BOAS. The displacement is also monitored by a dial indicator for calibration and video recording of the motion. Two thermocouples are mounted on the centers of SMA wires, one on the first wire along the airflow and one on the last wire near the air exit. Also the airflow temperature at inlet and outlet are monitored by two other thermocouples. The electric power is monitored by a DC current sampling resistor in the SMA wire circuit loop. The setup allows for testing the actuator with a comprehensive performance metric.

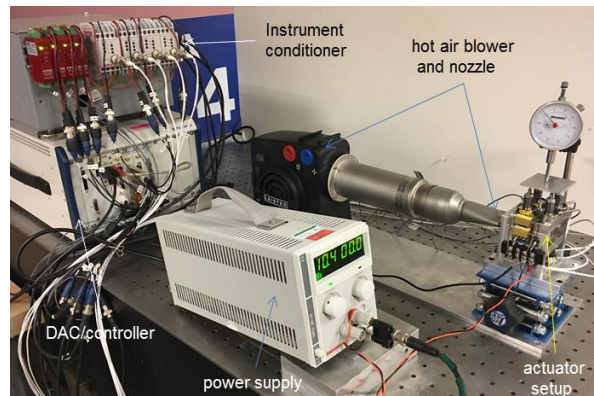


Figure 22 Tip clearance modulation test setup

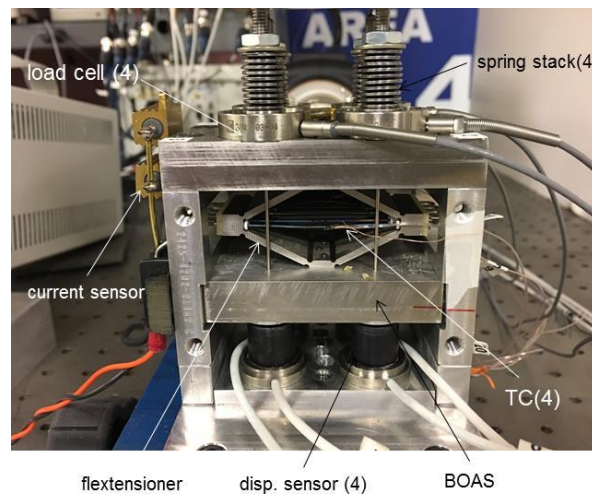
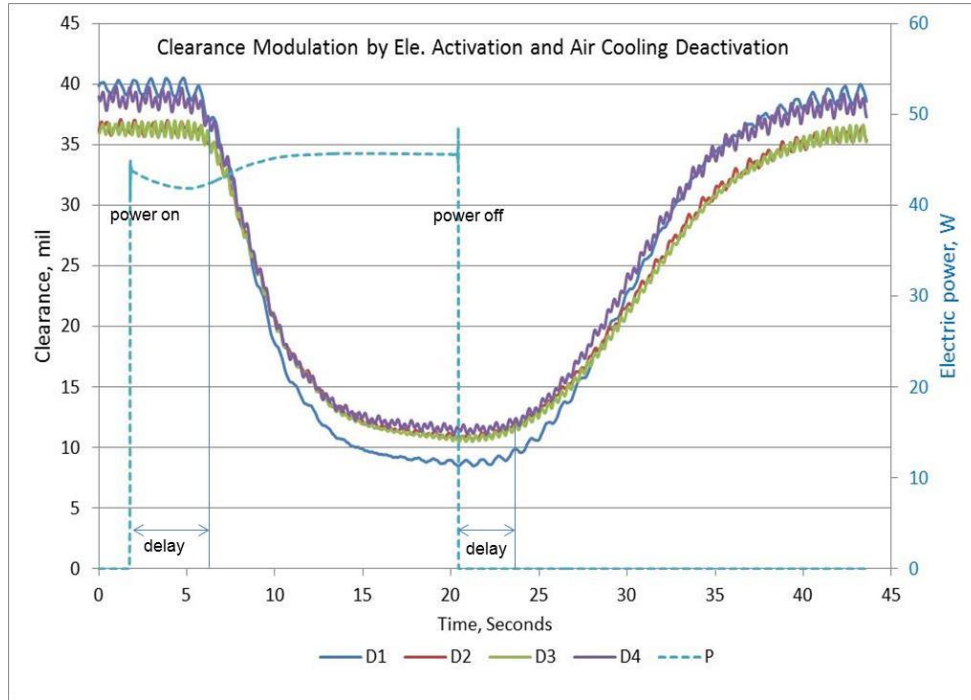


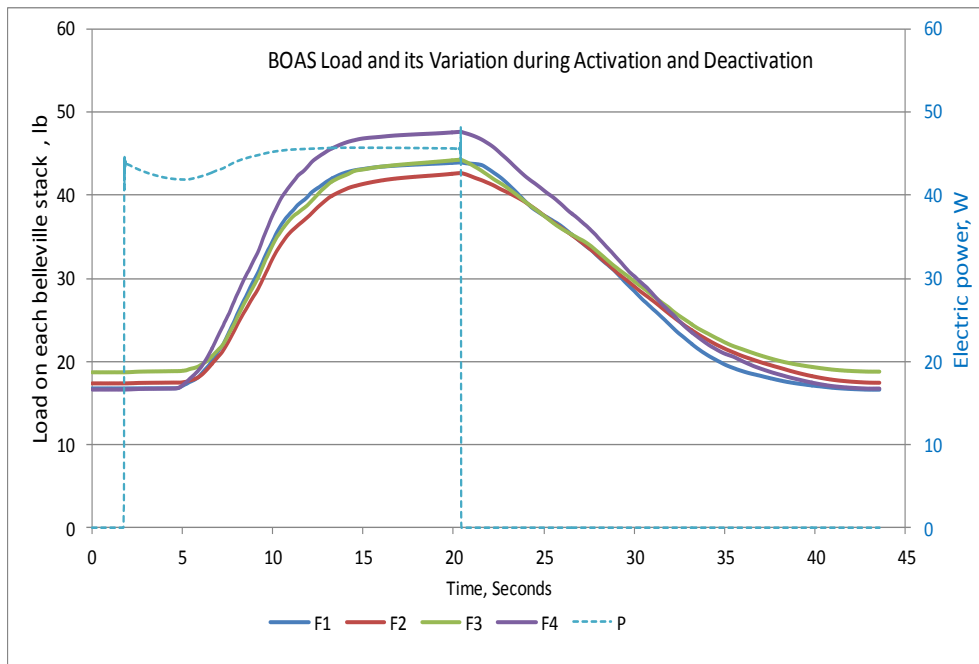
Figure 23 MTSMA truss actuator, BOAS, loading mechanism and instrumentation

Test Results and Analysis

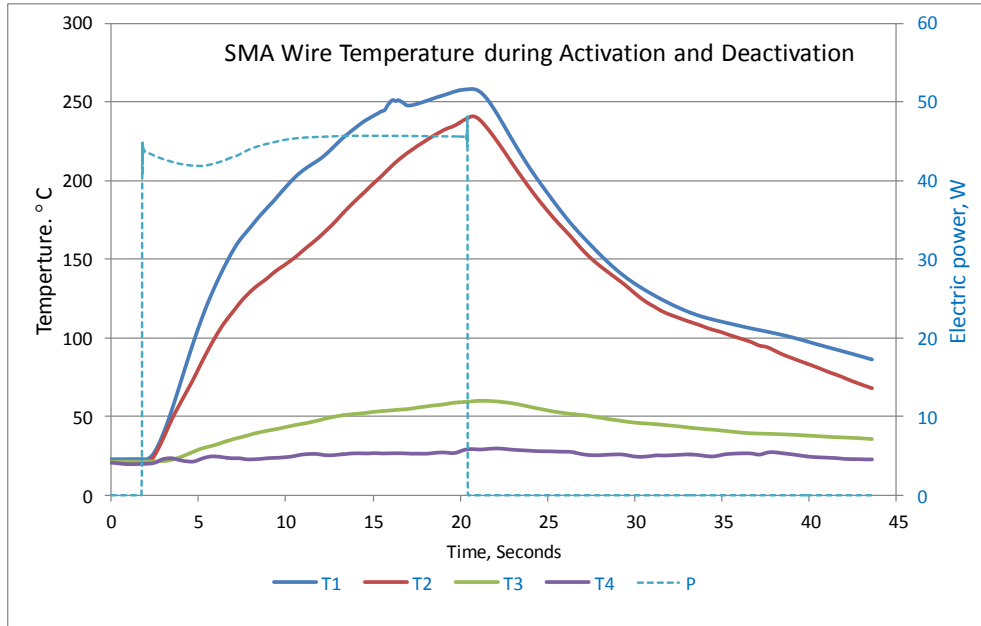
The actuator rig is tested in four different test conditions, and fourteen parameters are monitored in each test condition. Figure 24 through 25 graphically show the results in two test conditions (settings), the BOAS displacement and load at each corner, temperatures of the SMA wires and airflow inlet/outlet, and the electric power. Plots of two other conditions are not included but the crucial results are extracted and listed in the Table 2.



(a) Tip clearance at each corner of BOAS (D1~D4) and power P. Power on is: beginning of activation. Power off: beginning of deactivation.

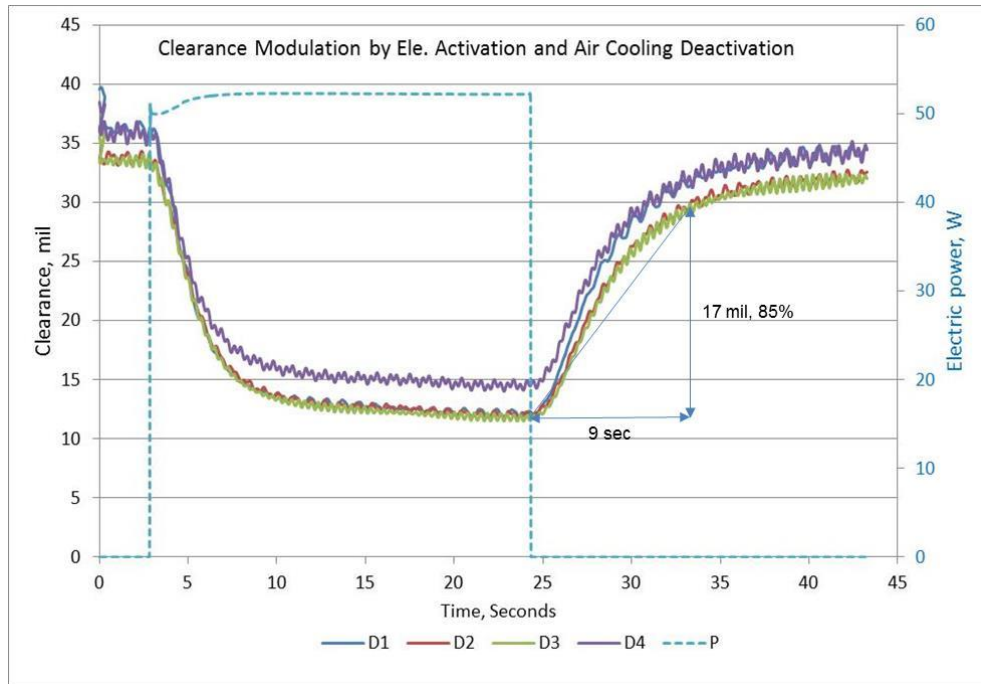


(b) Load on each corner of BOAS (F1~F4) and power P

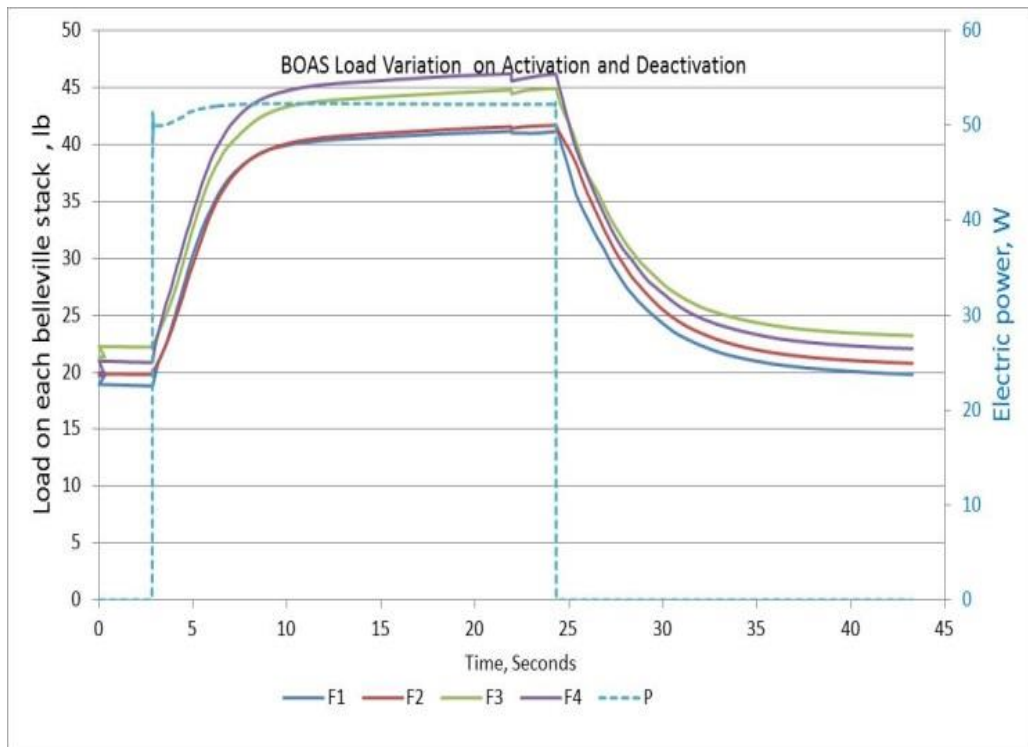


(c) Temperatures, wire #1 (T_1), wire # 4 (T_2), air inlet (T_3), air outlet (T_4)

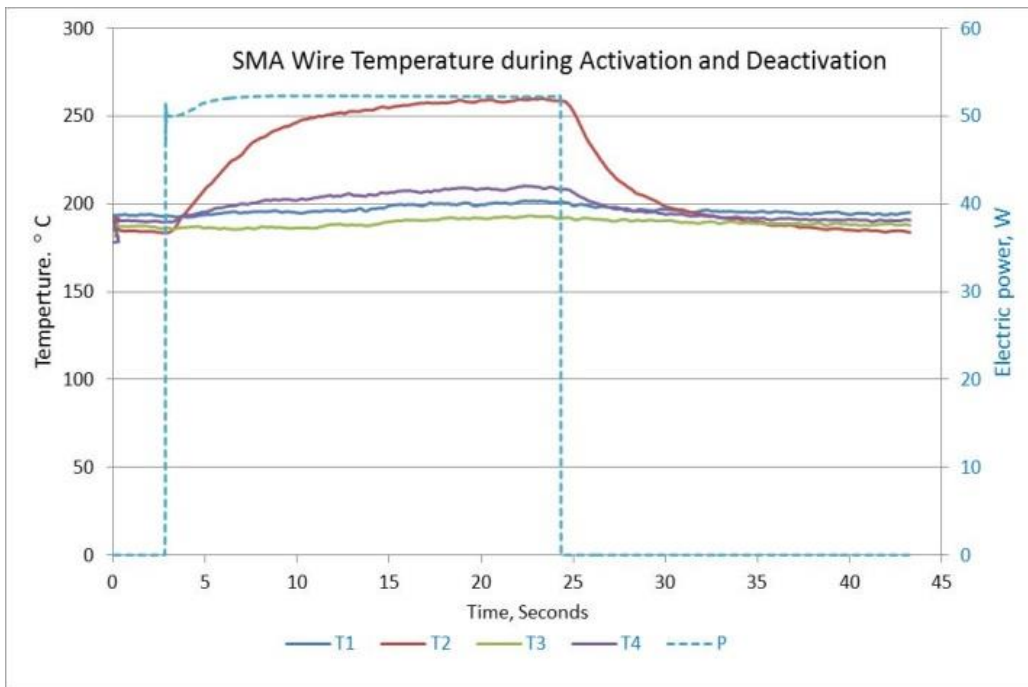
Figure 24 Test condition 1, 4 A current, 21 °C air temperature and 0.1 m/s airflow



(a) Tip clearance at each corner of BOAS (D1~D4) and power P. 85% of the clearance change is completed within the first 9 seconds.



(b) Load on each corner of BOAS (F1~F4) and power P



(c) Temperatures: wire #1 (T_1), wire # 10 (T_2), air inlet (T_3), air outlet (T_4)

Figure 25 Test Setting 4, 5A current, 180°C and 11 m/s airflow

Table 2 lists the four test conditions, control parameters and summary of the test results extracted from Figures 24 and 25, the numbers highlighted in green are more crucial than the others for the tip clearance control. The purples are the analytical prediction from the models (when available).

This document does not contain any export controlled technical data

	Setting 1	Setting 2	Setting 3	Setting 4
Airflow, speed, m/s	0.1	2.32	4.64	11.13
Airflow, temp, °C (normal)	21	130	170	180
Electric power, Watts	42	44	51	53
Bias load, lb	75	80	79	82
Tip clearance change, mil	25~30	23~25	22~23	21~23
Analytical	52			
Max load, lb, total/range	168/42~45	170/43~46	172/42~43	178/42~47
#1 SMA wire temp, °C	255	235	220	210
#10 SMA wire temp, °C	240	242	245	260
Air inlet temp, °C	21	135	165	179
Air outlet temp, °C	60	145	170	172
Time to open clearance, s	18	17	17	16
Analytical		(13)		(10)
Time to tighten clearance, s	14	16	18	24

Table 2 Test metric and summary of the test results

A few observations and conclusions can be made from these plots and Table 2 summary.

- 1) The response time of the full deactivation (widening clearance to the max) is in the range of 17 seconds for all the test conditions, approximately 5 times faster than the currently prevalent active case cooling (ACC) method. The majority of the clearance modulation (85% of the max) occurs within first 9 seconds (Figure 25 (a)). It is backed by the CFD simulation result with a reasonable agreement. This indicates that the most critical objective of the fast response clearance modulation is achieved by this design with good confidence.
- 2) The clearance modulation for all test conditions are within 0.021” to 0.030”, which meets or exceeds the requirement of 0.020”. However, the modulation are approximately 50% less than calculated with the model. It is believed that the loss of the stroke is caused by three factors. First, some HTSMA wire segments are unevenly heated so that they did not complete phase transformation during the heating and therefore, they did not at all or only partially contributes to the actuation, as qualitatively predicted by CFD model in Figures 16. Second, the HTSMA wires have relaxed or creped after many thermal and tension cycles, significantly reducing the strain recovery during the heating. Third, the slack is developed at the termination joints during the repeated operations which increasingly absorbs the wire strain recovery and reduces the net output.
- 3) Clearance and BOAS load response significantly lag the resistive heating for the airflow of room temperature (Figure 24(a)), even though the temperature rise and fall of the wires are in good sync with the power input. However, this lag tends to diminishes when the airflow temperature is raised (Figure 25 (a) and (b)). This indicates that there is detrimental backlash in the wire loop caused by insufficient pretension or bias. The airflow temperature rise results in pre-phase transformation contraction of the HTSMA wires and largely eliminates the “delay”.
- 4) The actuator demonstrates very stiff output characteristics and is capable of modulating the clearance against a significant mean load and variation. However, the larger than expected load variation during the thermal cycling indicates the combined spring stiffness of flextensioner and Belleville’s stack is too large and produces a total loading far from constant with BOAS movement.
- 5) The response time of the activation (heating to tighten clearance) is only slightly faster than the cooling, which appears not in agreement with CFD prediction even factoring the difference in the conditions (Figure 8(a) simulation, response time 2 seconds and 80 watts power vs the experimental 14 seconds and 50 watts power). Much more instantaneous power or a PID control is required to accelerate the heating if the actuation response time is also a consideration.
- 6) Binary actuation of the MTSMA is successfully demonstrated with the help of the mechanical stops. It is not possible to stabilize BOAS in any positions between two stops by adjusting the electric current.
- 7) BOAS driven by a single actuator at the center does not guarantee an even clearance modulation. A local asymmetric may occur at the corners which may result in unexcited rubbing with blades. Two actuators driving a BOAS in parallel appears a better configuration.

HTSMA material development

The objectives of the material aspect of the Phase II project are: 1) to identify and characterize medium-high temperature shape memory alloy MTSMA and fabricate into a user ready form for prototyping the tip clearance modulation device, 2) to investigate and identify a plausible material technology development path for the higher temperature shape memory alloys HTSMA with operating temperatures in excess of 600 °C toward the ultimate application to turbine environment was also sought.

These targets were successfully accomplished within the scope of the current project. $\text{Ni}_{49.2}\text{Ti}_{35.5}\text{Hf}_{15.3}$ alloy was identified as the best as high actuation authority MTSMA currently available. Its primary characteristics, the strain and stress relation under thermal cycle is shown in Figure 14. The material was hot rolled from ingot and then cold drawn into 0.030” diameter wire. They are then “trained” a few hundreds of thermal cycles to memorize their characteristic length before integrated into the clearance modulation actuator. The lab test shows this material is able to recover ~1% strain recovery under 350 MPa stress when heated above its Austenite finish temperature A_f . The actuator built with this wires is able to meet the stroke, force and response time target, as previously discussed.

Two other alloys $\text{Ni}_{10}\text{Ti}_{50}\text{Pd}_{40}$ and $\text{Ni}_{35}\text{Ti}_{30}\text{Hf}_{20}\text{Pd}_{15}$, were also identified and experimentally demonstrated to be potentially viable HTSMMA materials for the tip clearance modulation device. The preliminary differential scanning calorimetry (DSC) test, Figure 26, indicates the material can perform the desired actuation at temperature above 600°C, as shown by Figure 23. These material compositions are currently being refined and they are soon developed into useful forms such as rods, wires and ribbons. A full roadmap for manufacturing these higher-temperature shape memory alloys has also been established. The detailed work of the MTSMA and HTSMA material testing, manufacturing and training are given in Appendix.

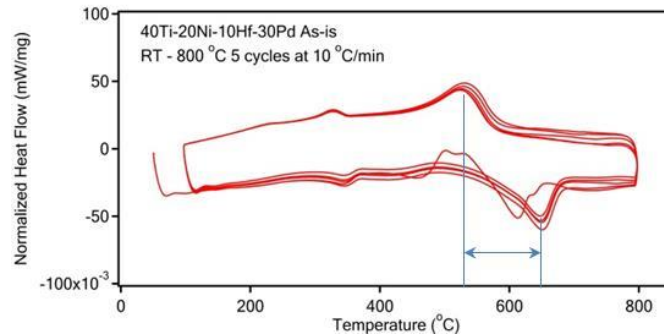


Figure 26 DSC plot of the HTSMA with phase transformation temperature 500~650°C in development

Summary

The twelve month research has explored a several concepts of wire truss actuator based electro-thermal tip clearance modulation methods. Among them, we have down selected one for full scale prototyping. The flextensioner MTSMA actuator was built, simulated and tested in a 180°C airflow environment and emulated air pressure load. It has demonstrated a satisfying performance and can meet the basic requirement of fast response time, adequate modulation stroke, variable load and very low power consumption for active clearance control. Both thermal-fluid model and testing show that such a thin wire based thermally active truss has very low mass density and is able to respond to the demand of sudden clearance change in a matter of 15 seconds. While the detailed design and testing process of a full scale prototype has revealed challenges in long term reliability and durability of MTSMA wires, it also indicates that it is in general a viable and ideal solution in structural compactness, compatibility, integratibility into turbine blade cavity.

The research also has completed a full scale investigation and search of MTSMA materials that are readily available for sampling and testing. One MTSMA material (220°C) was identified, successfully manufactured in

thin wire form and integrated in the actuation device. Another higher temperature SMA (~600°C) was also identified and preliminary characterization was conducted on small cubic sample. It shows a great promise for its ultimate implementation in the turbine. The road map toward its fabrication in useable form is established.

This research has gained us a confidence that the electro-thermal truss actuation as a fast tip clearance control method will find its way into the next generation turbofan engines that demand more fuel efficiency and less pollution in the near future.

Current TRL: TRL 4, completion of experimental validation and analytical evaluation with a bench top prototype,

Patent Applications

Two patent disclosures are submitted to USPTO.

- RRACC - Tip Seal with Electro-Thermal Actuation
- Thermal-Electric Fast Response Blade Tip Clearance Control Actuator

References

[1].Lattime, S. and Steinetz, B., Turbine Engine Clearance Control Systems: Current Practices and Future Directions, *Journal of Propulsion and Power* **20**, No. 2, March-April, 2004, *Journal of Propulsion and Power* **20**, No. 2, March-April, 2004.

[2].Kawecki, E. J, *Thermal Response Turbine Shroud Study*, Air Force Aero Propulsion Laboratory Technical Report, AFAPL-TR-79-2087, 1979.

[3].Ciokajlo, J. J., “Blade Tip Clearance Control Apparatus Using Shroud Segment Annular Support Ring Thermal Expansion,” U.S. Patent 5116199, 1992. *Ring Thermal Expansion,” U.S. Patent 5116199, 1992.*

[4].DeCastro, J. A., Melcher, K. J. and Noebe, D. R., *System-Level Design of a Shape Memory Alloy Actuator for Active Clearance Control in the High-Pressure Turbine*, 41st AIAA/ASME/SAE/ASEE Joint Propulsion Conference & Exhibit, 10 - 13 July 2005, Tucson, Arizona.

[5].DeCastro, J. A., Melcher, K. J., *A Study on the Requirements for Fast Active Turbine Tip Clearance Control Systems*, 40th Joint Propulsion Conference and Exhibit cosponsored by the AIAA, ASME, SAE, and ASEE Fort Lauderdale, Florida, July 11–14, 2004.

[6].Noebe, R.D., Draper, S.L., Nathal, M.V., Garg, A., *High-Temperature SMAs for Actuator Applications*, NASA Tech Brief, March 2008.

[7].Pratt and Whitney Internal Report (none-proprietary and not subject to ITAR control).

Appendix

Development, Training and Testing of Medium and High Temperature Shape Memory Alloys for Electro-Thermally Active Seals

Dr. Demircan Canadinc, Research Scientist

Dr. Ibrahim Karaman, Professor

BACKGROUND AND MATERIALS

The chemical compositions of the Medium Temperature Shape Memory Alloys (MTSMAs) and High Temperature Shape Memory Alloys (HTSMAs) fabricated within the scope of this project were determined to address some important issues regarding the utility of shape memory alloys at high temperatures and under cyclic loading. For instance, actuation fatigue is a common problem affecting shape memory alloys, and stems from dislocation generation during martensitic transformation, which significantly alters the stability of the alloy and leads to a notable loss of the actuation strain and accumulation of the total irrecoverable (remnant) strain (Figure 1).

Recently, NiTiPd alloys have been reported to be less prone to actuation fatigue as compared to other SMA systems (Figure 2) [Atli, PhD Dissertation, Texas A&M University, 2012], and thus, we selected some of our initial material compositions to contain Pd. Even though the NiTiPd alloys exhibit a better actuation fatigue performance, thermo-mechanical training of the SMA is still required in order to overcome the problem of loss of actuation strain upon cyclic loading. However, there is evidence that training of MTSMAs might be very difficult due to their high transformation temperatures (Figure 3) and as a result, the two-way shape memory effect might be difficult to achieve at these temperatures (Figure 4) [Atli, PhD Dissertation, Texas A&M University, 2012].

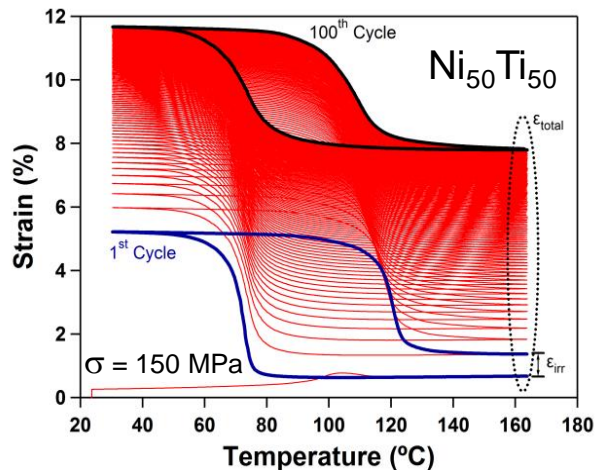


Figure 1. Loss of actuation strain and accumulation of remnant strain in equiatomic NiTi SMA [Atli, PhD Dissertation, Texas A&M University, 2012].

Quaternary alloying has been reported as one of the effective methods to improve actuation fatigue performance of SMAs and their stability at elevated temperatures (Figure 5) [Padula et al., AIAA, 2007]. Accordingly, we decided to add Hf to the NiTiPd system in order to achieve more stable actuation response. Hf was chosen since it

has been proven that the NiTiHf SMA system exhibits a very stable cyclic actuation response due to nano-precipitation hardening in the presence of Hf (Figure 6). Specifically, Ni is depleted from the matrix through nano-precipitation of the Ni-rich particles, which presents great flexibility in tailoring transformation temperatures and hysteresis.

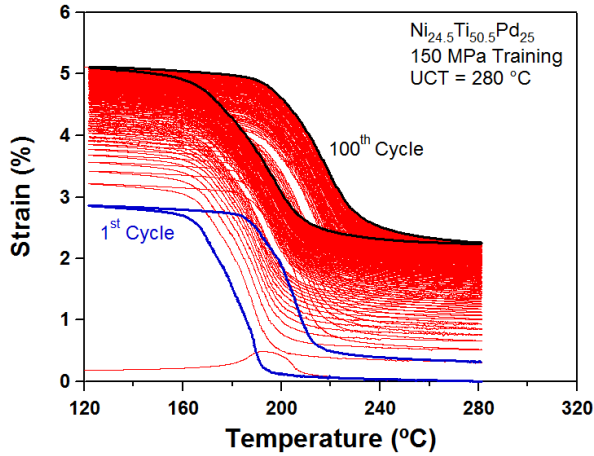


Figure 2. Actuation fatigue performance of NiTiPd₂₅ SMA [Atli, Karaman, Noebe. Materials Science and Engineering A, 2013].

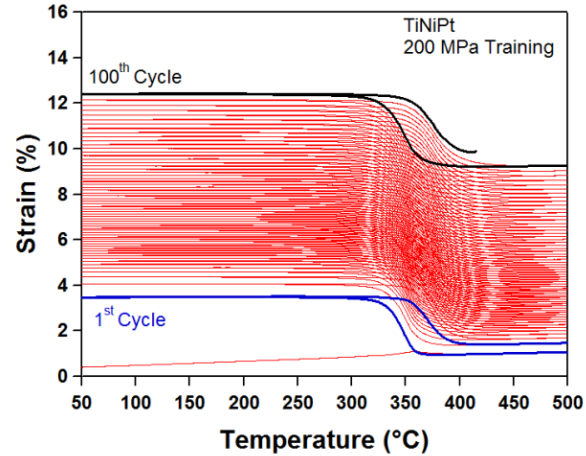


Figure 3. NiTiPt SMAs are difficult to train at elevated temperatures due to their high transformation temperatures [Atli, PhD Dissertation, Texas A&M University, 2012].

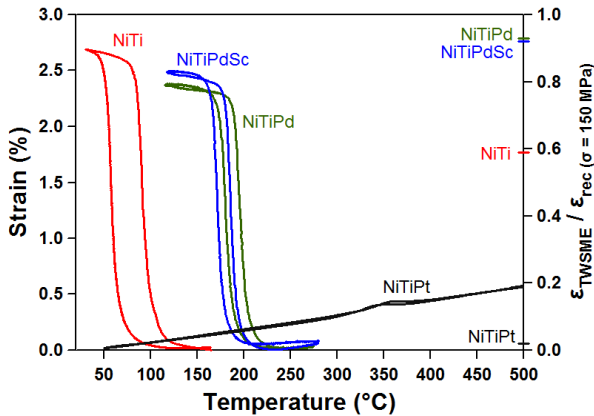


Figure 4. Two-way shape memory effect exhibited by NiTi, NiTiPd, NiTiPt and NiTiPdSc SMAs under zero stress, following training under 150 MPa for 100 cycles temperatures, demonstrating that it is difficult to achieve two way shape memory effect in SMAs with high transformation temperatures [Atli, PhD Dissertation, Texas A&M University, 2012].

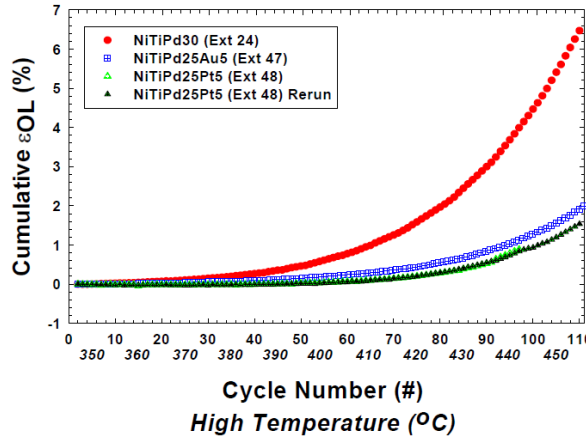


Figure 5. The effect of quaternary alloying on the actuation fatigue performance of high temperature SMAs [Padula et al., AIAA, 2007].

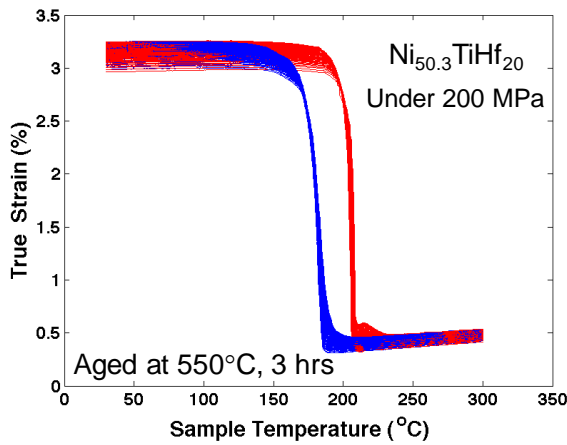


Figure 6. Stable actuation response of the nano-precipitation hardened NiTiHf₂₀ SMA [Courtesy of R.D. Noebe].

In this project, six different SMA compositions were selected and fabricated with the aim of achieving medium temperature range transformation temperatures (less than 400°C) and reasonable actuation fatigue response and functional stability. Furthermore, two of the selected and fabricated materials consist of quaternary alloying, i.e. NiTiPdHf alloys, which have not been studied before and expected to demonstrate good actuation stability. The selected alloys containing Ni, Ti, Pd and Hf were fabricated utilizing vacuum arc melting or vacuum induction melting techniques. The materials were cast in a controlled environment, and independent chemical content reports were obtained to prove the agreement between the fabricated and final chemical compositions. Furthermore, the compositions were also checked with the aid of wavelength dispersive spectroscopy (WDS) technique for consistency throughout the samples. All these materials were subjected to a series of initial characterization experiments, including WDS, scanning electron microscopy (SEM), optical microscopy (OM) and differential scanning calorimetry (DSC), as well as thermo-mechanical experiments to establish their phase transformation characteristics and mechanical properties. Specifically, alloys with the following chemical contents (in atomic %) were fabricated:

Alloy	Reason for Fabricating
Ni ₁₀ Ti ₅₀ Pd ₄₀	Transformation temperatures are around 400°C.
Ni _{50.3} Ti _{19.7} Hf ₃₀	This composition has not been studied before. Hf content was increased to 30% to achieve transformation temperatures around 400°C.
Ni ₃₅ Ti ₃₀ Hf ₂₀ Pd ₁₅	This composition has not been studied before. Pd is added to NiTiHf ₂₀ composition to increase the transformation temperature and enhance functional stability.
Ni ₃₂ Ti ₃₄ Hf ₁₆ Pd ₁₈	This composition has not been studied before. Pd and Hf contents were balanced to solve the potential issues, if any, with the cyclic stability of the Ni ₁₀ Ti ₅₀ Pd ₄₀ alloy.
Ni _{50.3} Ti _{29.7} Hf ₂₀	The samples of this composition already existed at Texas A&M University and were used to provide samples to UTRC at an early stage for them to test their design concepts at elevated temperatures, until one of the above alloy compositions are fully developed and samples are fabricated.
Ni _{49.2} Ti _{35.5} Hf _{15.3}	The samples of this composition already existed at Texas A&M University and were used to provide samples to UTRC at an early stage for them to test their

design concepts at elevated temperatures, until one of the above alloy compositions are fully developed and samples are fabricated.

Based on initial characterization experiments, three ($\text{Ni}_{49.2}\text{Ti}_{35.5}\text{Hf}_{15.3}$, $\text{Ni}_{10}\text{Ti}_{50}\text{Pd}_{40}$ and $\text{Ni}_{35}\text{Ti}_{30}\text{Hf}_{20}\text{Pd}_{15}$) of the six selected alloys were further mechanically processed and studied to examine their suitability for serving as MTSMAs ($\text{Ni}_{49.2}\text{Ti}_{35.5}\text{Hf}_{15.3}$) and HTSMAs ($\text{Ni}_{10}\text{Ti}_{50}\text{Pd}_{40}$ and $\text{Ni}_{35}\text{Ti}_{30}\text{Hf}_{20}\text{Pd}_{15}$). Thus, this report summarizes the results of experiments and processing procedures carried out on these three alloys for the sake of brevity. However, upon request, results obtained on the other materials will be made available to UTRC at any time.

MATERIALS CHARACTERIZATION

This section focuses on the initial characterization of $\text{Ni}_{49.2}\text{Ti}_{35.5}\text{Hf}_{15.3}$, $\text{Ni}_{10}\text{Ti}_{50}\text{Pd}_{40}$ and $\text{Ni}_{35}\text{Ti}_{30}\text{Hf}_{20}\text{Pd}_{15}$ alloys. Specifically, the results presented in this section were effective in determination of the processing of the materials and the test temperatures for the thermo-mechanical experiments. Characterization results in the post-processed states of the materials are presented in the corresponding sections.

Differential Scanning Calorimetry

DSC of $\text{Ni}_{10}\text{Ti}_{50}\text{Pd}_{40}$

The initial characterization of the fabricated alloys revealed that the $\text{Ni}_{10}\text{Ti}_{50}\text{Pd}_{40}$ alloy shows transformation temperatures around 400°C as indicated by the DSC results (Figure 7). Specifically, three consecutive cooling and heating cycles were run on the as-received sample, and the phase transformation behavior was demonstrated to be very stable (Figure 7). Consequently, the phase transformation temperatures for the as-cast $\text{Ni}_{10}\text{Ti}_{50}\text{Pd}_{40}$ were determined as:

Martensite start temperature (M_s): 400°C
 Martensite finish temperature (M_f): 375°C
 Austenite start temperature (A_s): 405°C
 Austenite finish temperature (A_f): 420°C

Following the initial DSC analysis, a heat treatment at 900°C for 1 hour was carried out on the as-cast samples under high vacuum, and the corresponding phase transformation response is presented in Figure 8. This heat treatment was applied in order to find a proper solutionizing heat treatment without altering the shape memory characteristics. It is apparent that the phase transformation behavior is stable following the selected heat treatment, yet the slight changes in the phase transformation temperatures is a strong indication of the need for plastic deformation for tailoring the microstructure of the material for the desired operating temperatures. Based on this conclusion, the as-cast material was hot-rolled, and the details of this procedure are provided in the corresponding section.

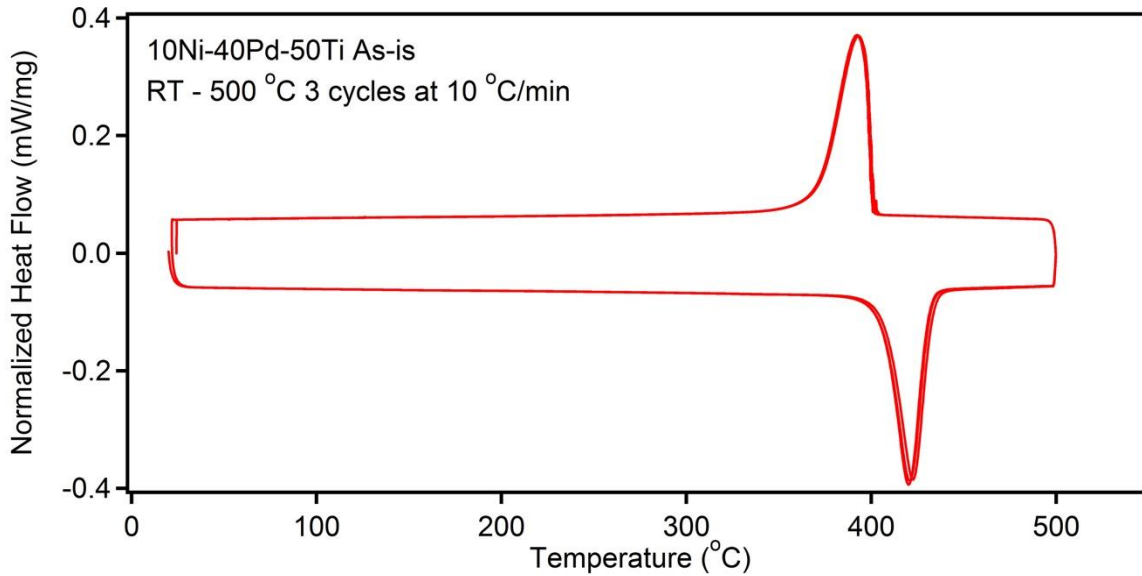


Figure 7. Three consecutive DSC cycles for the as-cast $\text{Ni}_{10}\text{Ti}_{50}\text{Pd}_{40}$ alloy.

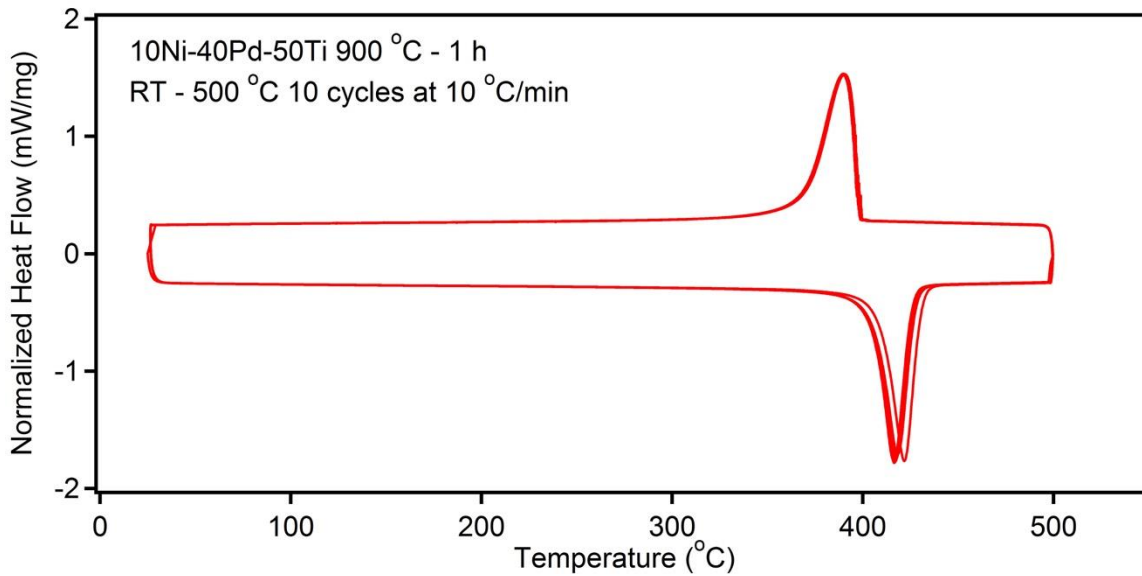


Figure 8. Ten consecutive DSC cycles for the $\text{Ni}_{10}\text{Ti}_{50}\text{Pd}_{40}$ sample heat treated at 900 °C for 1 hour.

DSC of $\text{Ni}_{35}\text{Ti}_{30}\text{Hf}_{20}\text{Pd}_{15}$

The DSC results of the as-fabricated $\text{Ni}_{35}\text{Ti}_{30}\text{Hf}_{20}\text{Pd}_{15}$ alloy indicated great potential for the utility of this alloy as a HTSMA (Figure 9). In order to ensure the repeatability, the DSC analysis was carried out on three companion samples (results are not shown), and the response was fully repeatable. The corresponding phase transformation temperatures for the as-cast $\text{Ni}_{35}\text{Ti}_{30}\text{Hf}_{20}\text{Pd}_{15}$ were determined as:

Martensite start temperature (M_s): 525 °C
 Martensite finish temperature (M_f): 470 °C
 Austenite start temperature (A_s): 537 °C

Austenite finish temperature (A_f): 686 °C

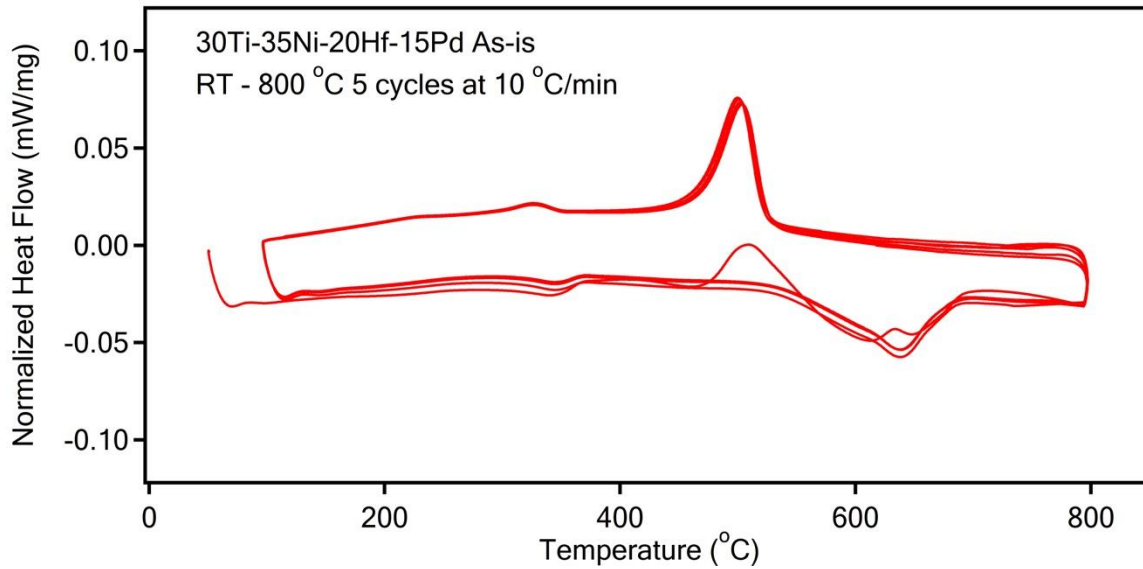


Figure 9. Five consecutive DSC cycles for the as-cast $Ni_{35}Ti_{30}Hf_{20}Pd_{15}$ alloy.

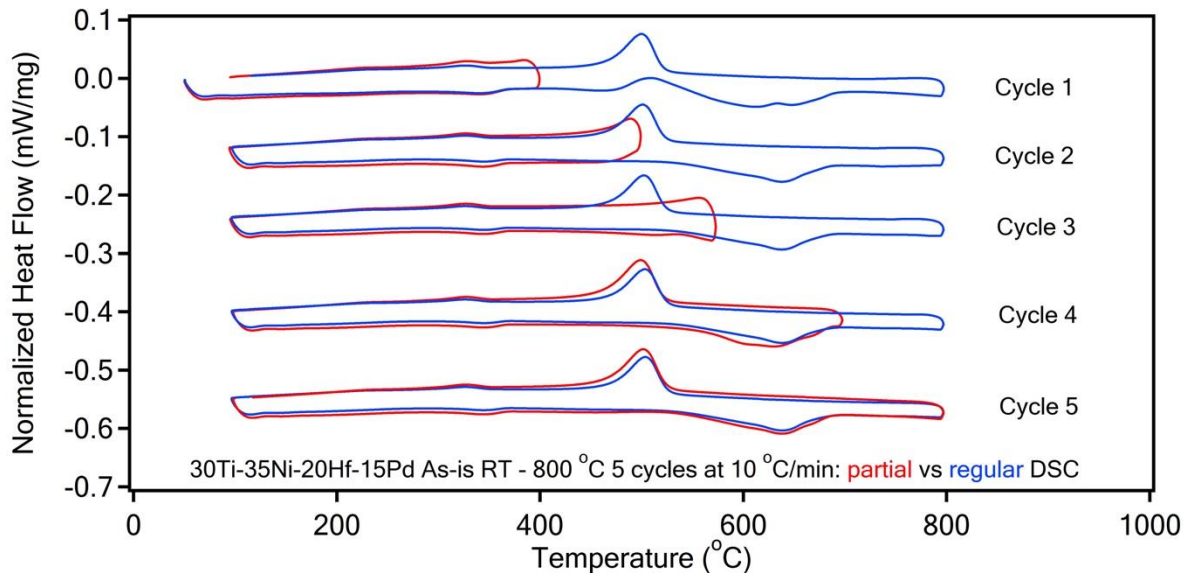


Figure 10. A comparison of the partial and full DSC analysis carried out on the as-cast $Ni_{35}Ti_{30}Hf_{20}Pd_{15}$ alloy.

In order to further analyze the DSC response and isolate the first cycle effect (the out of ordinary curve in Figure 9, which is typical for many SMAs), an additional partial DSC analysis was also carried out, such that the upper temperature for the heating cycle was increased cycle by cycle to quantify the phase transformation temperatures in a stepwise manner. A cycle by cycle comparison of the partial DSC results and the results of Figure 9 is presented in Figure 10. Accordingly, the observed behavior is not affected by the first cycle effect, and is repeatable and stable, as evidenced by the comparison.

DSC of $Ni_{49.2}Ti_{35.5}Hf_{15.3}$

The DSC results of the as-fabricated $Ni_{49.2}Ti_{35.5}Hf_{15.3}$ alloy indicated that this material is an ideal candidate for utility as an MTSMA (Figure 11). The corresponding phase transformation temperatures for the as-cast $Ni_{49.2}Ti_{35.5}Hf_{15.3}$ were determined as:

Martensite start temperature (M_s): 195 °C
 Martensite finish temperature (M_f): 170 °C
 Austenite start temperature (A_s): 240 °C
 Austenite finish temperature (A_f): 260 °C

It should be noted that, due to the presence of first cycle effect, the phase transformation temperatures were determined based on the second cycle.

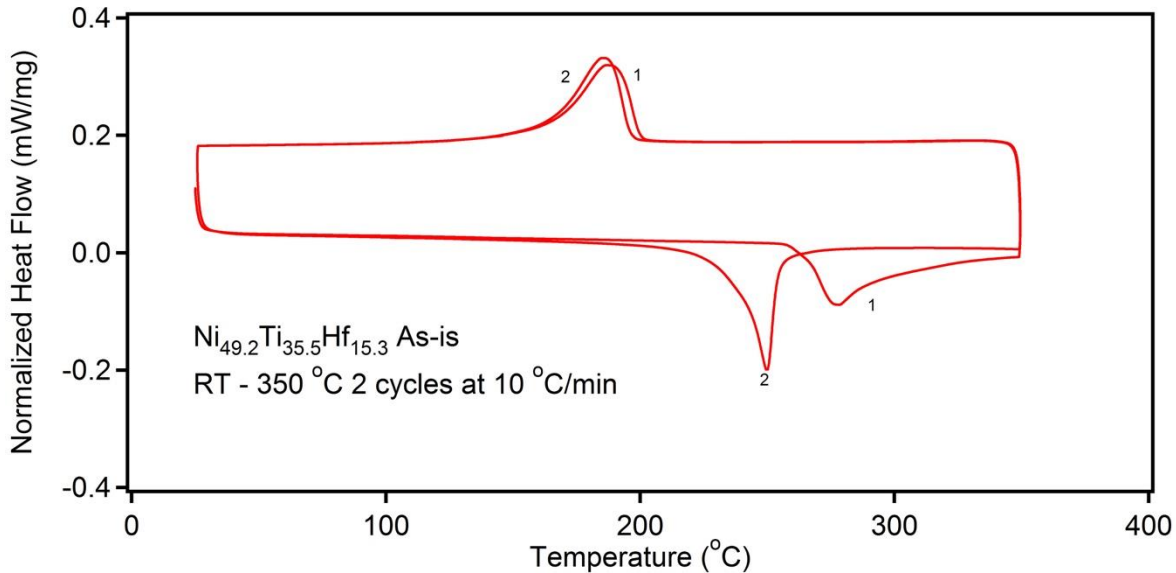


Figure 11. DSC for the as-cast $Ni_{49.2}Ti_{35.5}Hf_{15.3}$ alloy.

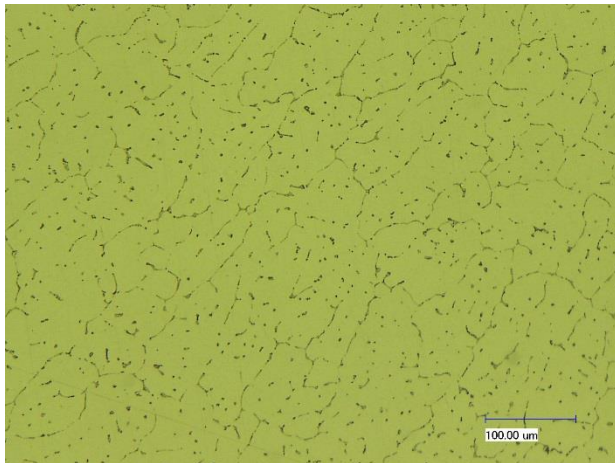


Figure 12. Optical Microscopy image showing the grain morphology and TiC particles in the microstructure of the as-cast $Ni_{10}Ti_{50}Pd_{40}$ alloy.

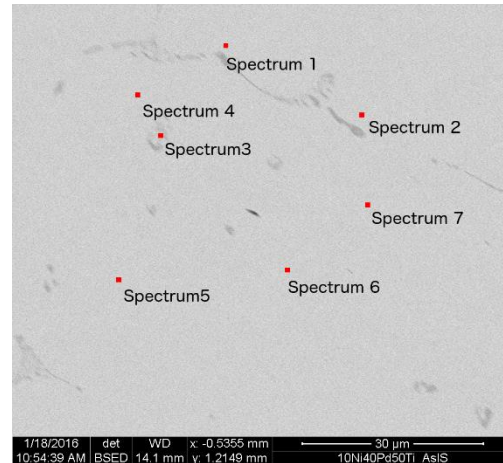


Figure 13. SEM image of the as-cast $Ni_{10}Ti_{50}Pd_{40}$ alloy. The EDS results of the indicated spectra are presented in Table 1.

Optical Microscopy

OM was utilized to check the surface quality of all samples as a precursor to SEM/EDS or WDS. Even though the fine details are mostly apparent under SEM, upon careful etching, OM can also reveal important information regarding the microstructure (e.g. grain size and orientations), and even the composition of the alloy (in terms of

uniformity of the phase(s) involved). For instance, the OM analysis of the Ni₁₀Ti₅₀Pd₄₀ alloy clearly showed that C-rich particles with elongated shapes, primarily decorating prior austenite grain boundaries, were prevalent in the as-cast form of this material (Figure 12). These are expected in NiTi based SMAs, which are TiC particles. This preliminary analysis implies the necessity of a proper thermo-mechanical processing for desolving, better distributing, and/or refining these particles, and refining the grain size for optimum shape memory performance. For this purpose, the as-cast Ni₁₀Ti₅₀Pd₄₀ alloy was subjected to hot rolling at 900 °C and with a thickness ratio of 5:1. The details of this process are provided in the corresponding section of the report.

Table 1. EDS analysis of the spectra indicated in Figure 13. All compositions are in weight %.

Spectrum	C	Ti	Ni	Pd
Spectrum 1	2.6	44.31	16.69	36.39
Spectrum 2	7.01	34.9	12.97	45.12
Spectrum 3	1.18	41.41	16.17	41.25
Spectrum 4	1.48	24.43	12.07	62.01
Spectrum 5		26.26	10.61	63.13
Spectrum 6		26.08	11.27	62.65
Spectrum 7		27.07	12.18	60.76

Scanning Electron Microscopy

SEM was utilized for detailed analysis of the material surfaces in the as-cast and processed forms. For instance, the distribution of the TiC particles within the austenite grains of the Ni₁₀Ti₅₀Pd₄₀ alloy is presented in Figure 13. An electron dispersive spectroscopy (EDS) detector in the SEM helped estimating the local chemical compositions of these particles and the surrounding matrix as shown in Table 1. These observations supported the decision to hot roll the Ni₁₀Ti₅₀Pd₄₀ alloy in order to dissolve the TiC particles and achieve a homogeneous microstructure for the sake of improved shape memory properties.

Another example to the utility of SEM is assessing the quality of the material surfaces upon processing. The 0.75 mm Ni_{49.2}Ti_{35.5}Hf_{15.3} alloy wires were carefully examined under SEM following drawing with the purpose of ensuring a high surface quality prior to training process. An example SEM image of the 0.75 mm Ni_{49.2}Ti_{35.5}Hf_{15.3} alloy wire surface is shown in Figure 14, demonstrating the absence of any undesired cracks or flows that would deteriorate the properties during training.

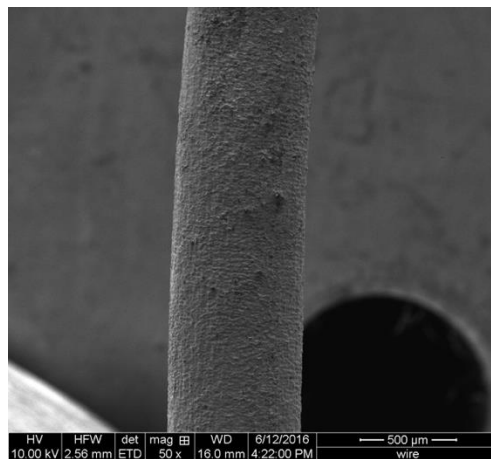


Figure 14. SEM image of the as-drawn 0.75 mm Ni_{49.2}Ti_{35.5}Hf_{15.3} alloy wire.

Wavelength Dispersive Spectroscopy

The WDS analysis was carried out on the $\text{Ni}_{35}\text{Ti}_{30}\text{Hf}_{20}\text{Pd}_{15}$ HTSMA in order to quantify the existing phases and particles in the microstructure. The backscatter electron (BSE) and secondary electron (SE) images presented in Figure 15 show that two different compositions are prevalent in the matrix as identified by bright (1) and dark (2) areas. Furthermore, precipitates/particles of both bright (3) and dark (4) intensities exist in the microstructure.

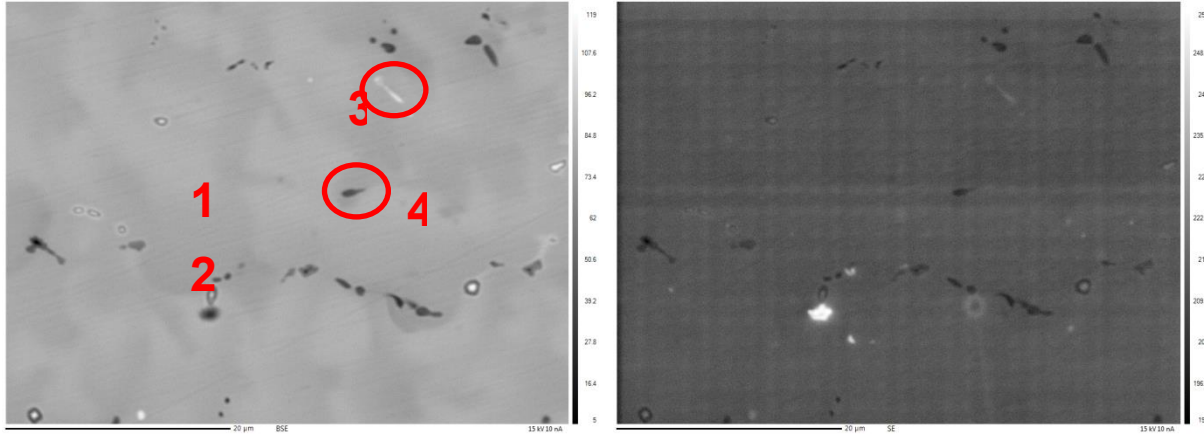


Figure 15. BSE (left) and SE (right) images of the as-cast $\text{Ni}_{35}\text{Ti}_{30}\text{Hf}_{20}\text{Pd}_{15}$ HTSMA.

A WDS scan of the corresponding surface revealed that the bright and dark regions in the matrix (Table 2), and the bright and dark precipitates (Table 3) are only slightly different than each other in terms of chemical composition. This is very important in terms of both validating the initially targeted chemical composition of the fabricated alloy and the uniformity of the matrix throughout the material. The verified uniformity of the matrix (despite the relatively small fraction of precipitates) implies that a stable actuation performance can be expected from this material during service.

Table 2. The WDS scan results of the matrix. The first 6 sampling points are located on the bright matrix (1 in Figure 15), and the last 6 sampling points are located on the dark matrix (2 in Figure 15).

Total	Ti	Ni	Pd	Hf	Zr	Total
100,00	29,57	34,52	15,42	19,58	0,91	100,00
100,00	30,05	34,66	15,22	19,25	0,83	100,00
100,00	29,00	34,70	15,44	19,96	0,89	100,00
100,00	29,11	34,65	15,45	19,98	0,81	100,00
100,00	30,08	34,55	15,10	19,49	0,79	100,00
100,00	29,64	34,50	15,36	19,61	0,89	100,00
100,00	30,68	35,03	14,94	18,45	0,90	100,00
100,00	31,00	35,24	14,64	18,23	0,89	100,00
100,00	31,17	34,55	14,81	18,48	0,99	100,00
100,00	31,06	34,88	14,74	18,41	0,92	100,00
100,00	30,32	34,75	15,20	18,83	0,91	100,00

100,00	29,96	34,71	15,20	19,25	0,88	100,00
--------	-------	-------	-------	-------	------	--------

Table 3. The WDS scan results of the precipitates (3 and 4 in Figure 15).

Ti	Ni	Zr	Pd	Hf	Total
55,64	26,63	0,89	6,53	10,30	100,00
56,63	26,84	0,88	6,37	9,29	100,00
55,73	26,60	0,93	6,54	10,20	100,00

PROCESSING OF MATERIALS

Hot Rolling of $\text{Ni}_{10}\text{Ti}_{50}\text{Pd}_{40}$

In order to dissolve the TiC particles in the microstructure of the $\text{Ni}_{10}\text{Ti}_{50}\text{Pd}_{40}$ alloy, the as-cast material was sliced via wire electro-discharge machining into the form of a 5.2 mm slab for hot rolling process. This slab was first jacketed in stainless steel in a high-purity argon environment in order to protect the material from oxidation during hot rolling. This jacket had to be renewed after each pass while trying to reach a thickness reduction ratio of 5:1, and the process was carried out at 900 °C, and a final product of 1.2 mm thickness was successfully obtained for potential wire drawing of the $\text{Ni}_{10}\text{Ti}_{50}\text{Pd}_{40}$ HTSMA.



Figure 16. Schematic demonstrating the rolling direction and the dimensions of the $\text{Ni}_{10}\text{Ti}_{50}\text{Pd}_{40}$ alloy slab that was hot rolled at 900 °C (left), and the final product of 1.2 mm thickness (right).

Following hot rolling, the $\text{Ni}_{10}\text{Ti}_{50}\text{Pd}_{40}$ alloy was examined with DSC (Figure 17), and the comparison of the results to those of the as-is and heat treated samples clearly show that the phase transformation properties were not altered at all upon processing.

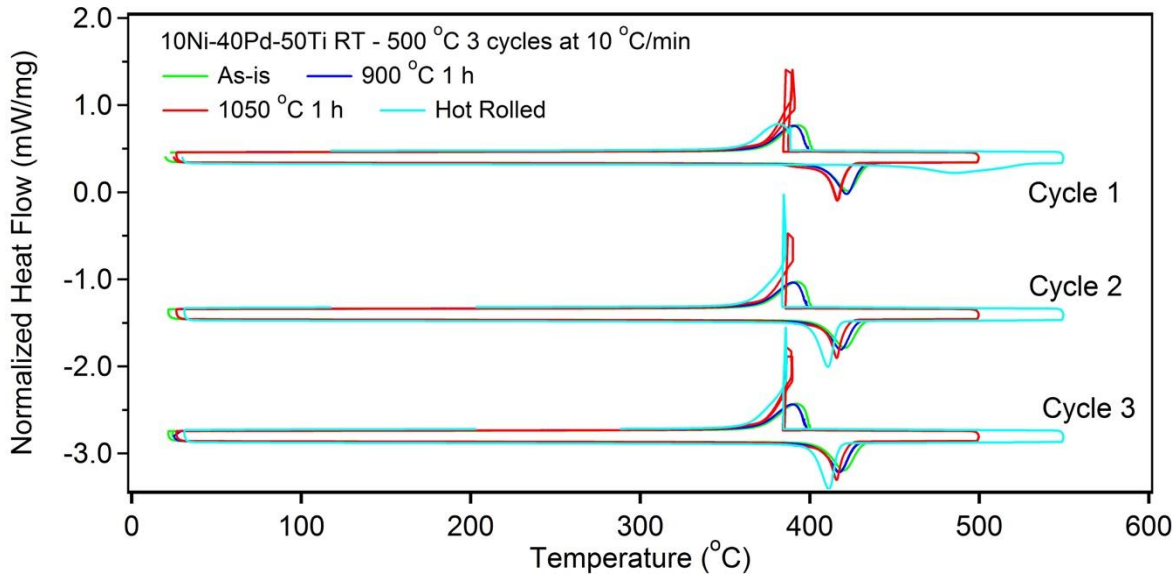


Figure 17. Comparison of the DSC results for the the as-cast, heat treated and hot rolled $\text{Ni}_{10}\text{Ti}_{50}\text{Pd}_{40}$ samples.

Hot Extrusion of $\text{Ni}_{49.2}\text{Ti}_{35.5}\text{Hf}_{15.3}$

The as-cast $\text{Ni}_{49.2}\text{Ti}_{35.5}\text{Hf}_{15.3}$ alloy was hot extruded at 900 °C in order to obtain the input material for the final wire drawing process. For this purpose, the as-cast $\text{Ni}_{49.2}\text{Ti}_{35.5}\text{Hf}_{15.3}$ alloy bar with a diameter of 12 mm was hot extruded at 900 °C to obtain 2 mm thick wire (Figure 18). The material was jacketed in stainless steel in order to protect the material from oxidation at elevated temperatures, and it was removed upon achieving a 6:1 reduction in diameter.

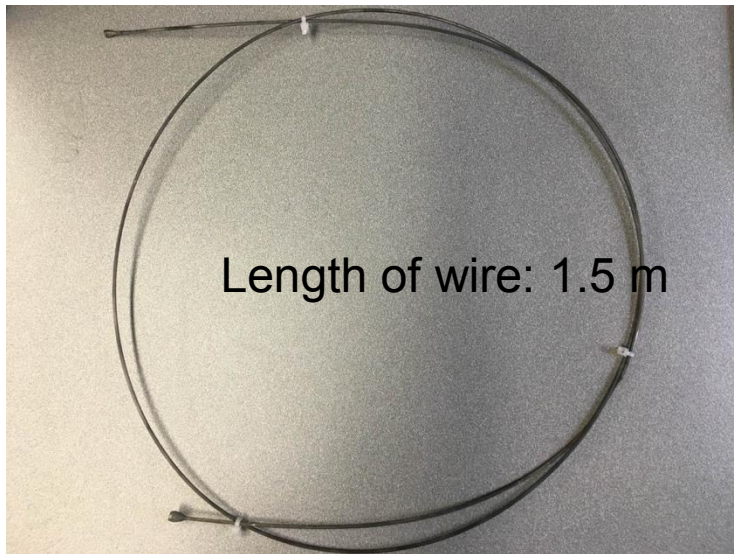


Figure 18. The as-cast $\text{Ni}_{49.2}\text{Ti}_{35.5}\text{Hf}_{15.3}$ alloy bar with a diameter of 12 mm (left) was hot extruded at 900 °C to obtain 2 mm thick wire (right).

The DSC of the hot extruded 2 mm wire in comparison to that of the as-cast material showed that the phase transformation response was relatively stable and unaltered upon hot extrusion (Figure 19). This result was encouraging for further processing, namely wire drawing of the hot extruded material.